UPPSALA
UNIVERSITET

Digital Comprehensive Summaries of Uppsala Dissertations from the Faculty of Science and Technology 1476

Annealing of $Cu_2ZnSn(S,Se)_4$ Thin Films

A Study of Secondary Compounds and Their Effects on Solar Cells

YI REN

ACTA
UNIVERSITATIS
UPSALIENSIS
UPPSALA
2017

ISSN 1651-6214
ISBN 978-91-554-9817-7
urn:nbn:se:uu:diva-314975

Dissertation presented at Uppsala University to be publicly examined in Häggsalen, Ångströmlaboratoriet, Lägerhyddsvägen 1, Uppsala, Friday, 31 March 2017 at 13:15 for the degree of Doctor of Philosophy. The examination will be conducted in English. Faculty examiner: Dr. Maarja Grossberg (Tallinn University of Technology).

Abstract

Ren, Y. 2017. Annealing of $Cu_2ZnSn(S,Se)_4$ Thin Films. A Study of Secondary Compounds and Their Effects on Solar Cells. *Digital Comprehensive Summaries of Uppsala Dissertations from the Faculty of Science and Technology* 1476. 85 pp. Uppsala: Acta Universitatis Upsaliensis. ISBN 978-91-554-9817-7.

Kesterite Cu_2ZnSnS_4 (CZTS) is interesting as a sustainable photovoltaic technology due to its earth-abundant elements and suitable semiconducting properties. To date, a record efficiency of 12.6% has been achieved but further improvements are required to reach high efficiency for industrial implementation. Among the limiting issues is the understanding of the annealing process, which is crucial in promoting high material quality. In particular, the knowledge of the effects of segregated secondary compounds on solar cell performance is lacking.

In contrast to formation of ZnS particles throughout CZTS film, it is notable that SnS forms and usually segregates on the CZTS top and rear surfaces. The influence of SnS on CZTS solar cells was studied by electron beam induced current measurements. It is found that SnS presence on the CZTS surfacecan introduce “dead area”, whereas it seems beneficial for solar cell current when accumulates on the CZTS rear. For SnS passivation and from investigation of the passivation effect from an Al_2O_3 thin layer at the CZTS rear, improvement in overall device performance could not be demonstrated, due to either poor CZTS bulk or non-optimal device structure. The limitation in CZTS bulk quality was shown from a thickness study where carrier collection saturated already about 700-1000 nm CZTS thickness.

Formation of SnS alongside CZTS implies the anneal is limited by a deficient sulfur partial pressure (P_{S2}). By looking into Sn-S phase transformations in SnS_2 films after annealing, we find that P_{S2} drops rapidly over the annealing time, which could be well-correlated to a series of changes in CZTS material quality including secondary phase formations and defect modifications. It is shown that annealing CZTS under sufficiently high P_{S2} is critical for CZTS solar cells with high open circuit voltage (upto 783mV was reached), possibly due to the defect modification.

Besides SnS, it is observed that Na_xS compounds are also readily formed on CZTS surfaces, due to Na diffusion from the glass substrate during annealing. Na_xS negatively affects the formation of the CdS/CZTS interface during chemical bath deposition. It can be removed by an oxidation process or wet chemical etching.

Keywords: Annealing, sputtering, thin film, CZTS, secondary phases, solar cell

Yi Ren, Department of Engineering Sciences, Solid State Electronics, Box 534, Uppsala University, SE-75121 Uppsala, Sweden.

ISSN 1651-6214
ISBN 978-91-554-9817-7
urn:nbn:se:uu:diva-314975 (http://urn.kb.se/resolve?urn=urn:nbn:se:uu:diva-314975)

谨献给我的家人和朋友
Till mina vänner och min familj
Dedicated to my friends and family

List of Papers

This thesis is based on the following papers, which are referred to in the text by their Roman numerals. Reprints were made with permission from the respective publishers.

I **Y. Ren***, J.J. Scragg, T. Ericson, T. Kubart, C. Platzer-Björkman, Reactively sputtered films in the $Cu_xS–ZnS–SnS_y$ system: From metastability to equilibrium, Thin Solid Films, 2015, 582, 208-214

II **Y. Ren***, J.J Scragg, C. Frisk, J.K. Larsen, S.-Y. Li, C. Platzer-Björkman, Influence of the absorber thickness on CZTS solar cell, Physica Solidi Status (A), 2015, 212(12), 2889-2896

III **Y. Ren***, M. Richter, J. Keller, A. Redinger, T. Unold, O. Donzel-Gargand, J. J.S. Scragg, and C. Platzer Björkman, Investigation of the SnS/CZTS interfaces in Kesterite Thin Film Solar Cells, in manuscript

IV B. Vermang*, **Y. Ren**, O. Donzel-Gargand, C. Frisk, J. Joel, P. Salomé, J. Borme, S. Sadewasser, C. Platzer-Björkman, and M. Edoff, Rear surface optimization of CZTS solar cells by use of a passivation layer with nano-sized point openings, IEEE Journal of Photovoltaics, 2016, 6(1), 332-336

V **Y. Ren***, N. Ross, J.K Larsen, K. Rudisch, J. J. S. Scragg, and C. Platzer-Björkman, Evolution of Cu_2ZnSnS_4 in non-equilibrium thermal processing with Quasi-in-situ Monitoring of Sulfur Partial Pressure, in manuscript

VI **Y. Ren***, J. J. S. Scragg, M. Edoff, J. K. Larsen, and C. Platzer-Björkman, Evolution of Na-S(-O) compounds on the Cu_2ZnSnS_4 absorber surface and their effects on CdS thin film growth, ACS Applied Material & Interfaces, 2016, 8(28), 18600-18607

VII J.K Larsen*, **Y. Ren**, N. Ross, E. Särhammar, S.-Y. Li, C. Platzer-Björkman, Surface modification through air annealing $Cu_2ZnSn(S,Se)_4$ absorbers, Thin Solid Films, 2016, in press

Personal Contributions to the papers

I Contributions to defining the project, all experimental work and material characterizations, data analysis, and writing with input from all co-authors

II All experiments, material characterizations, and all solar cell fabrications and characterizations, data analysis, and writing with input from all co-authors

III Responsible for the project, all experiments, most material characterizations, all solar cell fabrications and characterizations, data analysis, and writing with input from all co-authors. The EBIC was partly measured by Dr. Richter from Oldenburg University in Germany, and partly performed by Dr. Redinger from Helmholtz Zentrum Berlin in Germany, the SEM+EDS mapping is also partly performed by Dr. Redinger.

IV Contribution to developing the project, CZTS film fabrication (sputtering, annealing process and KCN etching), partly on the device fabrications and characterizations, discussion on data analysis and manuscript revision

V Responsible for the project, most experiments, all material characterizations, and all solar cell fabrications and characterizations, data analysis, and writing with input from all co-authors

VI Contribution to developing the project, all experiments except for KCN etching process, all material characterizations, and all solar cell fabrications and characterizations, data analysis, and writing with input from all co-authors

VII XPS measurements, discussion on data analysis and manuscript revision

Additional papers not included in the thesis

1. C. Frisk*, **Y. Ren**, T. Törndahl, J. Olsson, F. Annoni, C. Platzer-Björkman, On the extraction of doping concentration in Kesterite from capacitance-voltage: A Cu_2ZnSnS_4 and ZnS sandwich structure, in manuscript
2. O. V. Bilousov, **Y. Ren**, T. Törndahl, O. Donzel-Gargand, T. Ericson, C. Platzer-Björkman, M. Edoff and C. Hägglund*, Atomic Layer Deposition of Cubic and Orthorhombic Phase Tin Monosulfide, submitted
3. S. van Duran*, **Y. Ren**, J. Scragg, J. Just and T. Unold, Raman spectroscopy during high temperature annealing for In situ monitoring of Cu_2ZnSnS_4 synthesis, submitted
4. K. Rudisch*, **Y. Ren**, C. Platzer-Bjorkman , J. Scragg, Order-disorder transition in B-type Cu_2ZnSnS_4 and limitations of ordering through thermal treatments, Applied Physics Letters, 2016, 108(23), 231902
5. S. Li*, C. Hägglund, **Y. Ren**, J. Scragg, J. K. Larsen, C. Frisk, K. Rudisch, S. Englund, C. Platzer-Björkman, Optical properties of reactively sputtered Cu_2ZnSnS_4 solar absorbers determined by spectroscopic ellipsometry and spectrophotometry, Solar Energy Materials and Solar Cells, 2015, 149, 170-178
6. C. Frisk*, **Y. Ren**, S.-Y. Li, C. Platzer-Björkman, CZTS solar cell device simulations with varying absorber thickness, conference proceedings in Photovoltaic Specialist Conference (PVSC), 2015 IEEE 42nd
7. J. Márquez-Prieto*, **Y. Ren**, R.W. Miles, N. Pearsall, I. Forbes, The influence of precursor Cu content and two-stage processing conditions on the microstructure of $Cu_2ZnSnSe_4$, Thin Solid Films, 2015, 582, 220-223
8. J. K Larsen*, S.-Y. Li, J. J. S. Scragg, **Y. Ren**, C. Hägglund, M. D. Heinemann, S. Kretzschmar, T. Unold, C.Platzer-Björkman, Interference effects in photoluminescence spectra of Cu_2ZnSnS_4 and $Cu(In,Ga)Se_2$ thin films, Journal of Applied Physics, 2015, 118(3), 035307

9. J. K Larsen*, J. J.S. Scragg, C. Frisk, **Y. Ren**, and C. Platzer-Björkman, Potential of CuS cap to prevent decomposition of Cu_2ZnSnS_4 during annealing, Physica Solidi Status (A), 2015, 212(12), 2843-2849

Awards

1. Marie Curie Fellowship, ITN-KESTCELLS project, No. 316488, EU commission, 03/2013-03/2016

2. Best Poster Award, Material Research Society Spring Meeting 2015, San Fransisco, U.S.A. April, 2015

Contents

Abbreviations

PV	Photovoltaic
E_g	Bandgap energy
CIGS	$Cu(Ga,In)(S,Se)_2$
CZTS	$Cu_2ZnSn(S,Se)_4$
P_{S2}	Sulfur partial pressure
V_{Cu}	Copper vaccancy
Cu_{Zn}	Copper on Zinc antisite
Zn_{Cu}	Zinc on Copper antisite
Zn_{Sn}	Zinc on Tin antisite
Sn_{Zn}	Tin on Zinc antisite
SLG	Soda lime glass
V_{oc}	Open circuit voltage
q	Elemental charge
CBD	Chemical bath deposition
CBO	Conduction band offset
i-ZnO	Intrinsic Zinc oxide
AZO	Al doped ZnO
ITO	In doped SnO_x
J-V	Current–voltage characteristic
J_L	Light generated current
J_{sc}	Short circuit current
FF	Fill factor
η	Power conversion efficiency
J_0	Saturation current
k_B	Boltzmann constant
T	temperature
A	Ideality factor
R_s	Series resistance
R_{sh}	Shunt resistance
EQE	External quantum efficiency
IQE	Internal quantum efficiency
$\Phi_{AM1.5}$	AM1.5 solar spectrum
λ	wavelength
$a(\lambda)$	Absorption coefficient
w(V)	Space charge region width
L_e	Electron diffusion length in p-type CZTS
E	Energy
ÅSC	Ångström Solar Center
DC	Direct current
RF	Ratio frequency
XRF	X-ray fluorescence
XPS	X-ray photoelectron spectroscopy
XRD	X-ray diffraction
GIXRD	Grazing incidence XRD
SEM	Secondary electron microscopy
EDS	Energy dispersive x-ray spectroscopy
EBIC	Electron beam induced current
NR	Near infrared
UV	Ultra-violet
RT	Room temperature
PL	Photoluminescence
AE	Air exposure
AA	Air anneal

1. Introduction

1.1 Overview

Figure 1. The Wang Fu Jing neighborhood in Beijing before and after smog in Dec 2016 (The photo is kindly provided by Ms. Kerlijne Stessens)

In pace with the rapid development of modern technology as well as the growing global population, the demand for energy worldwide becomes more and more pressing. According to the International Energy Agency statistics 2016, the global energy consumption is approximately 125 trillion kWh (kilowatt hours), which is about 12.5% increase of the amount since 2010.[1] Up to now, the end-use energy consumption from electricity continues to grow fastest but the main energy generation worldwide is still predominantly from fossil fuel and coal. Utilization of these conventional energy sources has raised concerns on global warming due to greenhouse gas emissions in the past. In recent years in developing countries such as China and India, burning these sources for the exponentially increasing scale of industry has par-

[1] 2016 Key World Energy Statistics - International Energy Agency, page 28

tially caused deadly air pollution. *Figure 1* shows comparison of the air status in Beijing in December 2016 before and after the poisonous smog that contained high level of PM2.5.[2] Consequently, to prevent the increased negative effects from burning conventional energy sources, it is imperative to greatly strive towards development of clean energy by electricity from renewable and sustainable sources.

Among renewable energy sources for electricity, solar energy has shown strong advantages in its inexhaustible capacity. In particular, photovoltaic (PV) technology allows the generation of direct current that can be used directly by most electronics, presenting great potential for the trend in mobile energy as well as building integrated architecture. It has been predicted that the electricity generation from solar energy will grow 8.3%/year by 2040. This increased electrical power capacity by solar energy is expected to couple with a continuous cost reduction. On the basis of the learning curve predicted by International Renewable Energy Agency, the price of global average crystalline Si solar modules will be reduced by 22% for each order of magnitude cumulative production volume. By the year of 2014, the price has dropped to about 0.6 US$/W. To further reduce this cost, new materials for potentially high efficient solar cells need to be explored, and this thesis will be part of such a contribution.

1.2 Solar Cells

A solar cell, also named PV device, is a semiconductor device that converts light into electricity. Three processes are involved for this purpose: 1) Absorption of sunlight; 2) Generation of electron-hole pairs from the absorbed energy; 3) Collection of these carriers for external current. The basic working principle of the solar cell device originates from the utility of the photovoltaic effect as well as the formation of a p-n junction [1]. For this, solar cells are classically produced from solid semiconductor materials with the most common being Si. The first Si solar cell was publicly demonstrated in 1954 at Bell Labs.

Prerequisites to choose solar materials are the suitable bandgap (E_g) and absorption coefficient. As shown in *Figure 2*, the theoretical high efficiency

[2] PM2.5 refers to the particle pollution containing fine particle size below 2.5 μm. The chemical properties of the particles depend on the source of particles. PM2.5 is generally defined only based on the particles size that can potentially be dust, particulate matter, inhalable particles, smoke, and mist. PM2.5 is poisonous for the lung, throat and eyes. Exposure to high level of PM2.5 for short times can already start to initiate damage to human health. See the report "Health effects of particulate matter" by World Health Organization EU region.

solar cell resides in the bandgap energy spanning from 1.0 to 1.7 eV, with the 1st maxima at 1.38 eV and 2nd maxima at 1.15 and 1.6 eV. The bandgap of the solar absorber sets the threshold of the limit of the absorption of sunlight from the solar spectrum, whereas the absorption coefficient of the material determines the efficiency of light absorption. Therefore, material for solar absorbers with a direct bandgap (1.0 – 1.7 eV) and high absorption coefficient is mostly preferred. For this reason, thin film solar cell technology has been exploited in order to replace the Si solar cells, with potential lower cost for mass production.[3] State of the art thin film solar technologies are compared to Si in *Figure 2*, and it is demonstrated that chalcopyrite compound materials $(Cu(In,Ga)(S,Se)_2$ (CIGS) and CdTe) can be competitive to Si based PV technology [2].

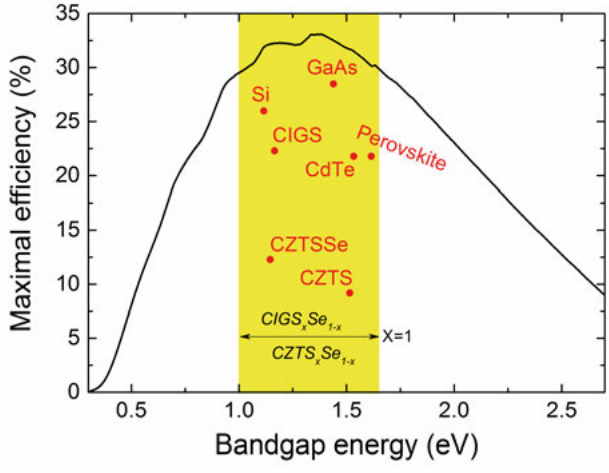

Figure 2 Efficiency limit for solar cells under illumination of AM1.5 solar spectrum; The yellow area shows the range of the bandgap of the solar material that could potentially yield highest efficiency. Examples of state of the art solar cells are indicated by the red dots [2]. Note that varying Ga/In and S/Se ratios can change the bandgap of CIGS material, while changing S/Se ratio can vary the bandgap of CZTS material, in the ideal bandgap regime.

Besides, another advantage of thin film solar cells is the flexibility of tuning the material bandgap. For example, via control of alloying Ga/In in thin film CIGS, as suggested in *Figure 2*, the absorber bandgap can be varied within the suitable energy regime for potential high efficiency solar cells. Barriers potentially limiting mass production of compound thin film technologies became increasingly discussed over the past years, and include 1) high mate-

[3] Thin film solar cells significantly reduce the thickness of the absorber material, for example, the required thickness for thin film solar cell is 1-4 μm, that is, about two orders of magnitude lower than Si. Besides, monolithic integration eliminates the need for extra series connection such as Ag used for Si.

rial cost for rare elements In, Ga [3-5]; and 2) the hazard of Cd to human health [6]. As an alternative, kesterite based material, namely $Cu_2ZnSn(S,Se)_4$ (CZTS), nowadays attracts considerable attention for research, due its potential to replace chalcopyrite PV with all earth abundant elements. Kesterite has similar crystal structure to CIGS, and shows a high absorption coefficient, a suitable direct bandgap energy (*Figure 2*: tunable bandgap energy by alloying S/Se ratio) and several appropriate semiconducting properties [7, 8], making it a promising candidate for the absorber material in a solar cell.

1.3 Aim of the Thesis

The broad target of this thesis is to develop the physical vapor deposition method for CZTS formation, in particular dedicating attention to the thermal processing of sputtered CZTS precursors. The focus is divided into two aspects. The first aim is to understand the secondary compound formation such as SnS and Na_xS, as well as the possible changes in CZTS bulk quality during the annealing process.[4] The second goal is to correlate material properties of annealed CZTS films with the final PV device performance. To do this, the investigation starts with the bulk CZTS material, and expands towards the front and rear interfaces of CZTS thin films, by using various material characterization techniques and device characterizations.

The thesis consists of three parts with 8 chapters in total. Chapter 2 briefly introduces fundamentals of CZTS material properties as well as the particular issues during its synthesis. Chapter 3 gives an overview of the architecture of CZTS solar cell integration, followed by presenting the most common methods to characterize and understand solar cell performance in Chapter 4. Chapter 5 explicitly describes the processes that were performed throughout the thesis work for CZTS thin film preparation and final solar cells. Afterwards Chapter 6 introduces the characterization techniques that were often performed to study the material properties of CZTS thin films and solar cells. Chapter 7 mainly summarizes the important results and discussions from the thesis work. At last, Chapter 8 presents conclusions of the thesis work and the outlook for future work on the kesterite based technology.

[4] It must be emphasized here that the term "annealing" used in this thesis work (and throughout the CZTS field), differs from the classical meaning of a long dwell time in inert or ambient environment, and rather refers to the general high temperature thermal process regardless of the gas atmosphere and process pressure.

2. Fundamentals

2.1 Kesterite – Cu_2ZnSnS_4 (CZTS)

Prior to diving into solar cell properties, primary material properties of kesterite will be discussed in this section. In this thesis work, the main focus is on the pure sulfide compound (CZTS), and analogous properties are expected for pure selenide compound CZTSe and alloyed S-Se.

2.1.1 Material Properties

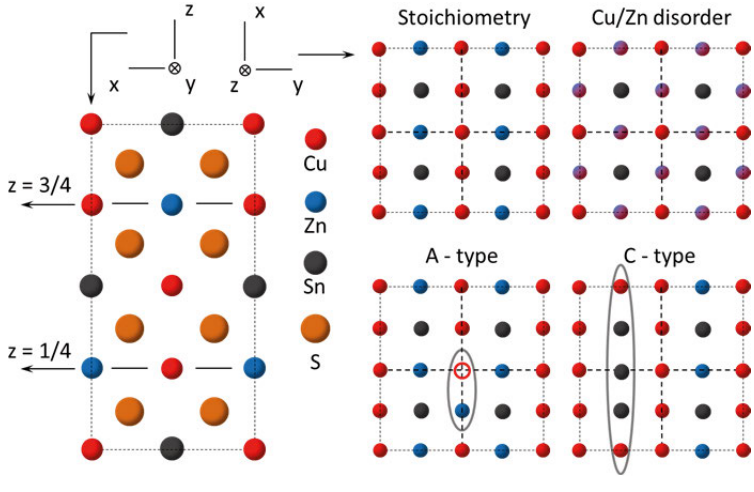

Figure 3. CZTS crystal structure and possible defect complex in the lattice; Cu/Zn cation disorder occurs on Cu-Zn planes (z=1/4 and 3/4); "A-type" and "C–type" defects respectively refer to (V_{Cu} + Zn_{Cu}) and ($2Cu_{Zn}$ + Sn_{Zn}) defect complexes.

A tetragonal unit cell of stoichiometric CZTS contains 16 atoms packed from two stacked zinc-blend unit cells (*Figure 3*). Tetragonal CZTS has been reported to have two possible structures, kesterite-type in *Figure 3* and stannite-type. In stannite-type, Zn atoms alternate with Cu atoms at z=0 and 1/2, while all sites at z=1/4 and 3/4 are occupied by Cu atoms. The difficulty to separate these groups is attributed to the similarity of Cu^+ and Zn^{2+} cation size, which makes common material characterization (such as x-ray diffraction) unable to resolve them. Neutron diffraction and theoretical calculations showed that kesterite-type is the most stable structure [9, 10].

The semiconducting properties of CZTS can be tuned by its composition. On one hand, alteration of the anion species can change the bandgap energy of the material from 1.6eV (pure sulfide) to 1.0 eV (pure selenide). On the other hand, shifting cation composition from stoichiometry to off-stoichiometry can potentially change the doping of CZTS material. A distinct concentration of the point defects can be formed because of variation in cation composition as were reported in both theoretical calculations [11, 12] and experiments [13], and these defects may be ionized to release free carriers. CZTS is a p-type semiconductor due to the predicted dominating point defects of Cu vacancy (V_{Cu}) and Cu_{Zn} antisite [11]. Nevertheless, in CZTS charged donor defects can be compensated by charged acceptor defects (a pair of positive and negative charge defects is named defect complex). These defect complexes are easier to form because of their lower formation energy compared to the isolated defects. The defect complexes can widen or narrow the bandgap [11]. *Figure 3* graphically presents examples of A-type (V_{Cu}+Zn_{Cu}) and C-type ($2Cu_{Zn}$+Sn_{Zn}) defect pairs in respective Cu-poor and Cu-rich CZTS.[5] Enhancement of A-type and V_{Cu} defects, because of Cu-poor and Zn rich composition, was predicted helpful for electrical properties of CZTS, whereas C-type and Cu_{Zn} defects, facilitated by Cu-rich and Zn-poor composition, could deteriorate CZTS solar cells. This has been used to explain why high efficiency solar cells are usually prepared with Cu-poor and Zn rich composition. In addition to defect complexes that are primarily altered by cation composition, the Cu/Zn cation disorder, occurring at z=1/4 and 3/4 of CZTS lattice in *Figure 3*, is less composition sensitive and is considered to be ubiquitous in CZTS compounds due to the similar cation size of Cu and Zn, as verified by theoretical calculations and experiments [11, 14, 15]. This defect pair can influence and be influenced by other defect constellations in CZTS as well ([16-18] and Paper V), thus affecting parameters of solar cells.

[5] Cu poor refers to Cu/Sn < 2 or Cu/(Zn+Sn) < 1, and vice versa. Zn rich refers to Zn/Sn > 1 or Zn/(Cu+Sn)>0.33, and vice versa. Sn rich refers to Zn/Sn < 1 or Sn/(Zn+Cu) > 0.33, and vice versa.

2.1.2 Phase Diagram of the Cu-Zn-Sn-S System

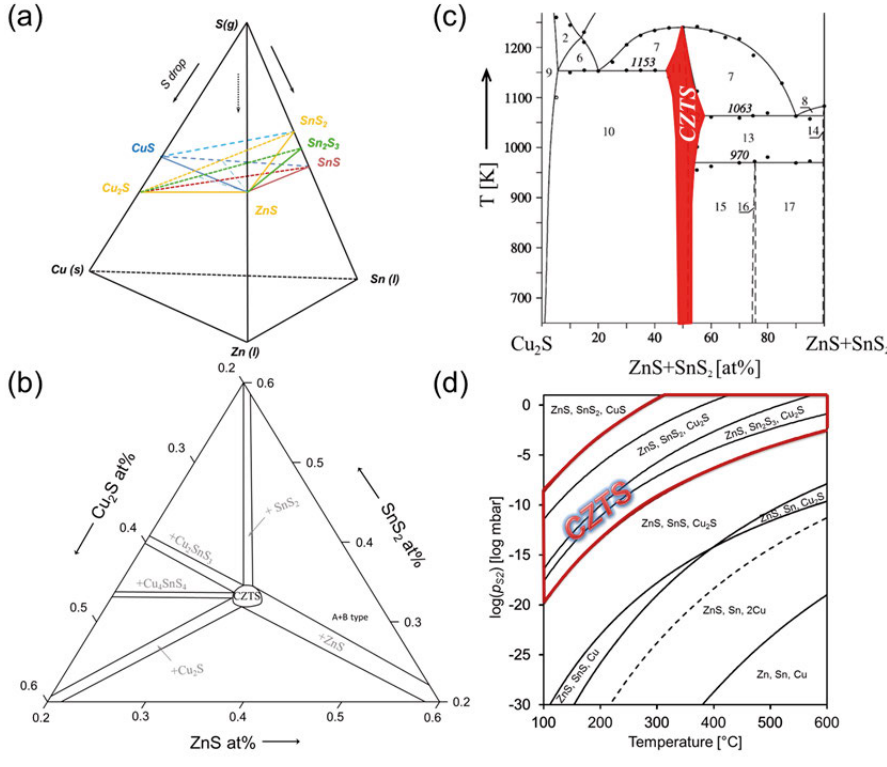

Figure 4. (a) Quaternary phase diagram of Cu-Zn-Sn-S system above 450 °C; (b) Isothermal section of Cu_2S-ZnS-SnS_2 system at about 400 °C [19]; (c) Temperature-composition phase diagram of the Cu_2S-(ZnS+SnS_2) mixture [19]; (d) Pressure-temperature phase diagram of Cu-Zn-Sn-S system [20];

A phase diagram is an important tool to study phases in grown material, in particular for the complex quaternary CZTS compound that is usually synthesized at high temperature (> 450 °C). *Figure 4a* displays the schematic of quaternary phase diagram of Cu-Zn-Sn-S system under standard pressure. It can be seen that cation composition, anion composition and process temperature are main variables for the system. When there is no change in sulfur partial pressure (P_{S2}), one can only consider temperature and composition of the material system, as shown in *Figure 4b-c*. From these two figures, it is notable that the CZTS single-phase region could be small, which only slightly widens when process temperature is above 700 °C. This means it is challenging to grow pure CZTS since trivial deviation of composition from the stoichiometry in CZTS system can trigger the formation of secondary phases.

2.1.3 Chemical Stability

One aspect making synthesis of pure kesterite material challenging is its chemical stability. A study combined with kinetic model and experiments by Scragg et al. shows that the decomposition process is driven by deficient P_{S2}, and thereby leading to the oxidation-reduction reaction of Sn in CZTS [21], as indicated in Eq.1. This process can be further exaggerated by the evaporation of the volatile SnS by-product (*Figure 4d*), and therefore it is expected that the decomposition process is firstly trigged close to CZTS surface (gas/solid interface).

$$Cu_2ZnSnS_4(s) \leftrightarrow Cu_2S(s) + ZnS(s) + SnS(s) + \frac{1}{2}S_2(g);\ SnS(s) \leftrightarrow SnS(g) \qquad \text{(Eq.1)}$$

As shown in *Figure 4d*, P_{S2} for CZTS decomposition is about in the order of 10^{-4} mbar at 590 °C, which seems to be much lower than widely used P_{S2} above 10mbar in practice. This could result from: 1) Non-equilibrium deposition process condition; 2) The validity of kinetic model. The later one becomes problematic for process 1) with highly mixed gas environment and 2) poor CZTS films that are not well grown or off stoichiometry in sulfur content. The former issue can come from 1) process design (graphite box, technical design of the process system); 2) Unknown gas status of sulfur polymorphs (S_2, S_4, S_6 and S_8). As a result, it becomes vital to monitor the true P_{S2} above CZTS surface in a thermal process. In paper I and V, it is shown that the P_{S2} could be monitored by examining a SnS_2 "monitoring film", which can be later correlated to a gradual change in material properties of CZTS films in the same annealing process.

$$2Cu_2ZnSnS_4(s) + Mo(s) \leftrightarrow 2Cu_2S(s) + 2ZnS(s) + 2SnS(s) + MoS_2(s) \qquad \text{(Eq.2)}$$

Besides CZTS surface decomposition, it has been shown that CZTS also tends to decompose at CZTS rear that is connected to the Mo back electrode (Eq. 2) [22]. However, this issue could be less significant when growing off-stoichiometric CZTS films at certain annealing conditions according to thermodynamic data (see *Table A1 in Appendix*). The chemical instability of CZTS surface and rear can be detrimental to CZTS solar cells, since they can lead to secondary phase formation at interfaces [23] as well as change of interface chemistry [24].

2.2 Growth of CZTS Film

2.2.1 Deposition Processes

Similar to chalcopyrite material, kesterite material can also be synthesized by either one-stage processes (i.e. directly grown on a substrate at relatively high temperature) or two-stage processes (i.e. deposition of CZTS precursor at low temperature followed by a high temperature annealing process), as summarized in *Table 1*. Currently, thermal co-evaporation (vacuum method) is the only way succeeding in a one-stage process. The polycrystalline CZTSe film is grown via evaporating elemental sources simultaneously onto a substrate with elevated temperature above 450 °C. However, the low process pressure as well as the cold chamber wall makes it difficult to control chalcogen partial pressure [24]. The best CZTSe solar cell processed from this method is about 9.2% efficient so far [25]. To resolve the problem of insufficient P_{S2} and to promote better crystal quality of CZTS film, high temperature thermal processes were introduced as a second-stage [24, 26]. The adaptation of thermal processes offers great flexibility of synthesis routes for CZTS precursor (both vacuum and non-vacuum methods as presented in *Table 1*). Because of this, parameters of the thermal process have to be carefully adjusted to connect to the nature of CZTS precursor films.

Table 1. Summary of reported process to synthesize CZTS film

One-stage	Thermal evaporation (>450 °C)	
Two-stage	Thermal evaporation [27], sputtering[28], co-sputtering[29, 30], reactive co-sputtering[31, 32], monograin[33]	Rapid thermal process[28], tube furnace[26], hotplate[34]
	Spin coating[34], electrodeposition[35]	(all above 450 °C)

In general, it has been reported that annealing of kesterite precursors is often conducted in the temperature range of 450-600 °C, with a typical dwell time below 2h [29, 30, 36-43]. In addition, a chalcogen excess environment provided by either elemental vapor source or H_2S/H_2Se gas is almost always supplied during the process. Understanding the annealing process for kesterite is a challenging task, since numerous physico-chemical processes may occur individually, successively or at the same time, such as diffusion [26], impurity incorporation [44, 45], chemical reaction [43], formation of secondary phases [32], CZTS decomposition [46], CZTS recrystallization, CZTS grain growth, etc.. Each one of them or their combinations could potentially change electrical properties of CZTS solar cells [23, 47-49]. To acquire better understanding of CZTS synthesis at high temperature and to

correlate to solar cell performance, it is important to minimize and precisely control the variables during the annealing process. Nowadays the two-stage process has led to significant improvement in kesterite solar cells, e.g., efficiency of CZTSe solar cell fabricated from thermal co-evaporation process has been enhanced from 8.9% to 11.6% [50, 51]. Until now the two-stage process is believed to be the most successful route to prepare kesterite thin film, holding record efficiency of 12.6% solar cell devices published in literature.[6] State of the art CZTS solar cell performance fabricated from various deposition methods can be found in *Table A2 in Appendix*.

2.2.2 Formation of Secondary Compounds

Secondary phase formation is a key issue that seems inevitable for growing CZTS films. It primarily originates from off-stoichiometric composition of the CZTS film, as demonstrated by the phase diagrams in *Figure 4*. Nevertheless several other factors can enhance this process, including: 1) surface [21] and back contact decomposition [52]; 2) Alkali driven phase separation and formation [45, 47]; 3) Variation in precursor deposition methods such as metal/compound stacking layers [43], intentional Zn-rich surface termination [53], etc.; A summary of secondary phases has been reported by Altamura and Vidal [54]. In short, according to the binary phase diagrams and theoretical calculations [55, 56], cubic $Cu_{1.8}S$ [49], monoclinic Cu_2SnS_3 [20], hexagonal SnS_2 [56], orthorhombic SnS [32, 57] and cubic ZnS are the most common and favorable phases to form at the typical processing temperature ranges of 450-600 °C for CZTS. Note that it is not unusual to have other distinct crystal structures for these phases, particularly if the process conditions are non-equilibrium. A summary of secondary phases and their removal methods is listed in *Table 2*.

Table 2. Formation and removal of the secondary phases in different stoichiometric CZTS

Composition	Secondary phases	Removal method	Ref
Cu-rich	Cu_xS, Cu_xSnS_y	KCN (Cu_xS)	[49]
Zn-rich	ZnS	HCl	[58]
Sn-rich	SnS_2, SnS	$(NH_4)_2S$ or thermal evaporation	[59]

Formation of Cu_xS phase is very common under Cu-rich condition. It was considered that melting Cu_xS phase at high temperature could assist the grain growth for chalcopyrite material. However, this effect is not reflected in CZTS when the Cu_xS capping layer was used on top of Cu-poor CZTS [49].

[6] A 13.7% efficient CZTSSe device was announced at the 26th PVSC in Singapore 24-28th of October 2016 without further details.

Besides, Cu rich conditions can vastly increase the doping of CZTS, which has proven to be detrimental to solar cells [11, 49, 60]. As a result, growing CZTS with a Cu-poor condition, Zn rich and Sn rich composition is currently most widely pursued. For this, formation of ZnS and Sn_xS_y phases are often reported during the growth of CZTS films.

ZnS is usually found to distribute spatially within CZTS films with the most being at front and rear interfaces [32]. The influence of ZnS phases at CZTS interfaces on solar cells has been reported by an intentional control of the Zn flux via thermal evaporation [53]. It was observed that segregation of ZnSe is harmless on the backside of CZTSe but detrimental on the surface of CZTSe. This was later supported by another study where a pure ZnS buffer was deposited on top of CZTS [61]. Unfortunately, effects on solar cells from the ZnS phase in bulk CZTS are rarely reported because of the difficulty in complete elimination of this phase.

In contrast to ZnS, the influence of Sn_xS_y phases on CZTS solar cells is less studied. Formation of these phases is in close relation to CZTS formation, since they can form not only due to the composition of the film but also because of the change in P_{S2}. Sn_xS_y can be observed on surface and rear of the CZTS film. By now a wet removal process was developed to study its influence on CZTS solar cells but it is unclear if the electrical properties of the CZTS film is simultaneously affected by such etching treatment [59]. As one of the main topics for this thesis work, studies on Sn_xS_y phases are specifically performed (Paper I, II III and V). The impact of Sn_xS_y on CZTS solar cells is investigated via electron beam induced current measurements (Paper III). In addition, the Sn_xS_y phase is also found to be useful for monitoring P_{S2}, which can be correlated to alterations in CZTS material qualities (Paper I and V).

In addition to the above overviewed phases that are inherent from Cu-Zn-Sn-S system, the actual secondary phases can also involve broader species such as Na related compounds, elemental chalcogen species and oxides. These extra compounds can modify surface and grain boundary properties of CZTS film hence the ultimate solar cells in different manners, as later discussed in paper VI and VII.

3. CZTS solar cells

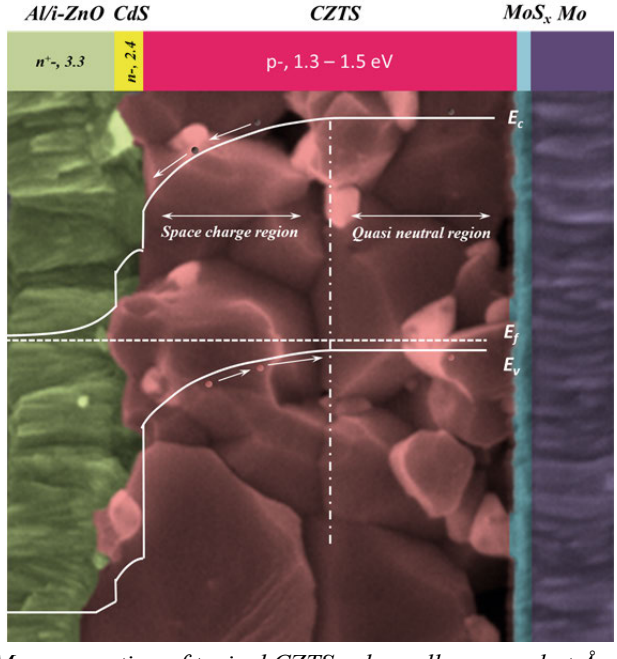

Figure 5. SEM cross section of typical CZTS solar cell prepared at Ångström Solar Center, overlayed by a schematic of the band diagram of a CZTS solar cell

The most common structure of CZTS thin film solar cells is shown in *Figure 5*, including (from right to left) Mo back electrode, p-type CZTS absorber, n-type CdS buffer layer and n^+-type ZnO based emitting layer (window layer). The CZTS solar cell is substantially composed of hetero p-n junction, and the respective band diagram under thermal equilibrium is sketched as white curves. On one hand, since the window layer is highly n-type doped, the space charge region is considered to be extended towards absorber bulk. On the other hand, since the bandgap of window layer is higher than the absorber layer and the thickness of buffer is much thinner, the visible light is expected to be mostly absorbed into the CZTS layer. Therefore, the quality of the absorber as well as the interfaces next to absorber layer is crucial for device performance. In the ideal case, the CZTS/Mo interface (or CZTS/MoS_x interface of annealed CZTS films) is expected to be less defec-

tive and to present ohmic behavior, so that the transport of majority charge carriers towards back electrode can proceed smoothly, while minority charge carriers can be collected without high recombination velocity. As to CZTS/buffer interface, a small spike-like band offset is preferred since it may increase the energetic barrier for recombination of minority carriers thus improving the open circuit voltage of the solar cell. In this section, state of the art development on CZTS stack layers will be briefly introduced.

3.1 The Substrate

1-3 mm thick soda lime glass (SLG) is widely exploited as the substrate in kesterite technology. In addition to mechanically supporting the rest of the solar cell stack, SLG can also release Na, which is demonstrated essential to guarantee good solar cell performance, to CZTS film during the growth process [44, 62]. Nowadays alternative mechanically flexible substrates are also highly motivated to promote mobile solar energy and building integrated capability. The potential roll-to-roll deposition is more compact and can be much more time effective for lower cost. Reports have shown that ZrO_2 [63], stainless steel [64] and enamel ceramics [65] can be these candidates yielding reasonable device performance above 6%. It is notable that CZTS films grown on alternative substrates will require an external addition of Na.

3.2 The Back Contact

The back contact is used as the transition layer between substrate and absorber layer, as indicated by purple and cyan colors in *Figure 5*. It requires several properties:

- Compatible mechanical properties with the substrate and later deposited absorber, such as thermal expansion coefficient
- Allowance for Na transport that is fed by SLG
- Low contact resistivity and sheet resistivity
- Possibly resistive to corrosive chalcogen environment during the high temperature process

A Mo layer of about 300-1000 nm thickness is the most widely employed back contact in kesterite solar cells, since it is proven to be successful in chalcopyrite technology by fulfilling most prerequisites commented above. In CZTS, Mo can easily react with chalcogen species during high temperature annealing process, leading to formation of $MoS(Se)_x$ interlayer between

CZTS and Mo. Nevertheless, it is still debated whether $MoS(Se)_x$ is electrically harmful to kesterite solar cells [51, 66, 67], since the reported carrier transport within CZTS film varies from one research group to another, making it difficult to conclude if back contact recombination or series resistance induced by $MoS(Se)_x$ is crucial to solar cells. In paper II, by varying absorber thickness and combining with SCAPS 1D simulation [68], we found that the back contact recombination did become severe for the ultra-thin CZTS solar cells, suggesting that the CZTS/MoS_x rear interface could not be ideal.

To control the formation of $MoS(Se)_x$ layer, several approaches have been explored such as deposition of thin passivation layer on top of Mo or establishment of multi-Mo layers. In the first approach, passivation layer, such as TiN [51], TiW [69], TiB_2 [70], carbon [71] etc., have been tested and reported. However, none of them shows significant advantage over bare Mo layer. In paper IV, we used thin nanosized-opened Al_2O_3 as the passivation layer above Mo, and showed that the passivation effect may be beneficial for ultra-thin CZTS solar cell [62]. The disadvantage of introducing a passivation layer lies in limiting the Na supply and adding extra non-optimal interfaces in the solar cell structure. As an alternative, the approach of building multiple Mo layers is proposed, which includes intentionally depositing a sacrificial top thin Mo layer for $MoS(Se)_x$ formation to prevent further consumption of the Mo film.

3.3 The CZTS Absorbers

The polycrystalline CZTS absorber film is the core of the solar cell stack in which the incoming sunlight will be absorbed and converted into output power. Hence, the CZTS layer is required to have good conductivity for charge carrier transport. Specifically, the excited electrons in CZTS by incoming photons should have long lifetimes as well as good mobility for sufficient diffusion length, and the net charge carrier concentration in CZTS should be controlled. The ultimate goal is to minimize the probability of the charge carrier recombination before they are collected. It has been reported that the charge carrier lifetime for CZTS is typically below 13 ns [29, 72] and the carrier diffusion length is less than 500 nm [60, 68]. In contrast, the carrier lifetime and diffusion length for CZTSe are typically below 7 ns and about 2000 nm [50, 73], respectively. Hence, the short circuit current extracted from selenide based kesterite PV devices normally is not an issue.

Nevertheless, a common bottleneck for CZTS based solar cells is the high open circuit voltage (V_{oc}) deficit ($E_g/q–V_{oc}$), and the higher the CZTS bandgap energy, the larger V_{oc} deficit appears [74]. Exact reasons for this matter remain open, and it is still unclear what the true bandgap of CZTS is.

It is proposed that effects from interface recombination as well as band tailing caused by potential fluctuations in bulk CZTS are the main origins [74, 75]. As to the contribution from interface recombination, attention is focused on improving band alignment, and it was shown that alternative buffers such as (Cd,Zn)S could reduce the V_{oc} deficit by about 90 mV [76]. Reasons for band tailing are attributed to charged defect constitutions in bulk CZTS, among which Cu/Zn cation disorder is considered most likely due to its low formation energy [11]. However, recent studies have shown, although the reversible process of the Cu/Zn cation order-disorder transition can contribute to the bandgap narrowing up to 200 meV [77], the V_{oc} deficit could remain uninfluenced [78]. Therefore, other deep defects or defect interactions may be responsible for the V_{oc} deficit. To passivate or alternate these potential defects, intense research focus is nowadays turned to alkali doping [79, 80] and metal alloying like Ge and Cd [81, 82] in CZTS. Furthermore, efforts on compositional gradients [83] and air annealing [84] are also attempted for CZTS thin film in order to boost the overall efficiency.

3.4 The Buffer Layer

Similar to CIGS/CdTe technology, chemical bath deposited CdS (CBD-CdS) has been widely applied as the buffer layer for CZTS solar cells. The chemical bath usually is mixed with Cd precursor (CdI_2, $CdSO_4$, $CdCl_2$ or $Cd(Ac)_2$), thiourea (S precursor), ammonium hydroxide as well as deionized water. The basic reaction route of CBD-CdS on the CZTS substrate can be generalized by

$$2Cd(NH_3)_4{}^{2+} + SC(NH_2)_2 + 2OH^- \rightarrow CdS + CN_2H_2 + 4NH_3 + 2H_2O \qquad \text{(Eq.3)}$$

As a result, increasing Cd salt concentration and thiourea concentration, increasing the pH of the solution as well as the bath temperature can promote the formation of CdS particles. The actual reaction process behind Eq.3 is still under debate. It is generally accepted that the growth of CdS is catalyzed by $Cd(OH)_2$ adsorbed on the substrate surface, which facilitates the so called atom-by-atom growth. The advantage of the atom-by-atom growth is to allow a precise control of the CdS thickness. As illustrated by the solid curve in *Figure 6*, the growth rate by atom-by-atom process can be controlled accurately in the linear region (B). Nonetheless, once the homogeneous growth where the CdS particles form in solution and precipitate at the surface becomes dominant, the atom-by-atom growth of CdS will shift into the agglomerated CdS growth, which can result in uncontrollable and porous overlayer, as displayed in the upper electron microscopy image in *Figure 6*. The agglomeration growth of CdS can be quickly initiated at the very beginning of the CBD process if the parameters of the solution are quite off from

an optimal condition. This can be a particular issue for the CZTS surface with the presence of Na_xS compound, since this can alter local pH close to solution/CZTS interface (Paper VI).

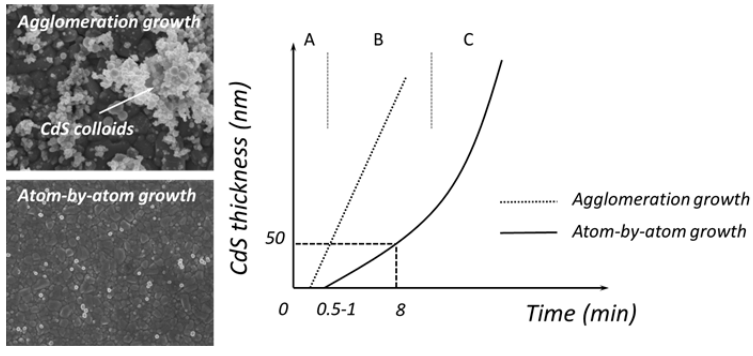

Figure 6. Schematic of a typical growth curve of chemical deposited CdS film with two different growth mechanisms at ÅSC (right): (A) Incubation period (B) Linear growth of a compact CdS layer (C) Rapid growth of a porous overlayer by coagulation of CdS particles from solution. The dash curve shows an exemplary growth curve of CdS film when the initial chemical bath condition deviates from an optimal condition. SEM images of CZTS film on which CdS film is deposited under different mechanism (left)

Until now the introduction of a CdS buffer layer on top of CZTS films still seems crucial for functional solar cells. Ericson et al., have shown that a complete replacement of CdS layer with ZnO layer leads to nonfunctional solar cell [61]. Several reasons for the role of CBD-CdS have been proposed, including protection of CZTS surface from sputtering damaging during the ZnO deposition, cleaning of surface compounds on CZTS surface, incorporating Cd into Cu poor CZTS surface [29], reduction of optical reflection, etc.. However, a major problem of using CdS for CZTS is the non-ideal conduction band offset (CBO) CZTS/CdS. As presented by the band diagram in *Figure 5*, the cliff-like CBO can potentially lower the barrier for charge carriers to recombine at the interface.[7] Besides, another concern of using CdS lies on its hazard to human health. Consequently alternative buffers are explored in order to replace CdS, which includes SnO_x [85], ZnO_xS_{1-x} [61], $Zn_xSn_{1-x}O_y$ [86] and In_2S_3 [87]. Nonetheless, by far the highest open circuit voltage (783 mV) of CZTS solar cell is still based on CdS buffer ([33] and Paper V).

[7] The slight spike-like CBO at CZTS/buffer is the most favorable band structure for CZTS solar cells. The spike-like CBO should not be too large so that the electrons can still be thermally emitted across the buffer. The non-optimal CBO can be a reason for decreased open circuit voltage of thin film solar cells.

3.5 The Window Layer

The window layer is consisting of two parts: resistive intrinsic ZnO (i-ZnO) and conductive Al-doped ZnO (AZO). The i-ZnO layer is deposited in between Al-ZnO and CdS layers, in order to prevent shunt paths across CZTS film. The AZO is the front electrode that is highly doped. It should provide maximum lateral electrical conductivity with highest optical transmission. To reduce the free carrier absorption at long wavelengths, the conductive window layer is preferred to have low free charge carrier concentration but high mobility. For this purpose, In-doped SnO_x (ITO) is also often used as the conductive window layer instead of AZO, but the cost is higher than AZO.

4. Solar Cell Characterization

4.1 Solar Cell Operation

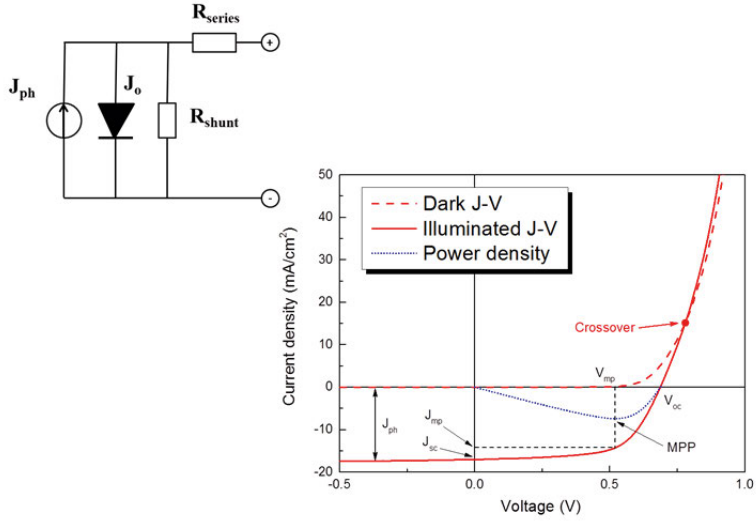

Figure 7. Typical current density – voltage (J-V) characteristics of a solar cell operated under dark and one sun illumination; the left corner shows the equivalent circuit of solar cells during these operations.

The performance of a solar cell is usually characterized by a current–voltage (J-V) curve. To better understand this electrical behavior, the operation of a solar cell is often assumed equivalent to an electrical circuit drawn in *Figure 7*. Without intentional illumination, a solar cell is substantially a p-n diode. Its J-V behavior can be described by the first part of Eq.4 in *Table 3* and is indicated by the dashed line in *Figure 7*. Under standard illumination (25°C, AM1.5 solar spectrum and an input power of 100 W/cm^2), a constant current density should be generated by an ideal solar cell due to 100% carrier collection. Therefore, the entire J-V curve will be shifted downward by J_L, as expressed in Eq. 4 in *Table 3* and presented in the solid curve in *Figure 7*.

Nevertheless, this shift approximation is rarely applicable for thin film solar cell and a crossover of dark and light J-V curve is often found.[8]

The solar cell parameters extracted from the illuminated J-V curves are short circuit current (J_{sc}) at zero voltage, V_{oc} at zero current and fill factor (FF). The FF is to measure how close to the product of V_{oc} and J_{sc} that a solar cell can operate at its maximal output power point, as summarized in Eq.5 in *Table 3*. The FF can be affected by series and shunt resistances that are shown in the equivalent circuit (*Figure 7*), leading Eq. 4 changing to Eq.6 that is known as the one diode model. In Eq. 6, the quality of the diode, i.e. the ideality factor A (A=1 for an ideal solar cell), is also considered. Assuming the shunt resistance is high enough so that the second term of Eq.6 becomes negligible, V_{oc} can be mathematically expressed in Eq. 7. Ultimately, the last parameter, i.e. the power conversion efficiency, of the solar cell can be calculated according to Eq.8.

Table 3. Summary of numerical equations that are applied to characterize solar cell performance

Equation	Formula	Remarks
Eq.4	$J = J_0(\exp(qV/k_BT) - 1) - J_L$	J_0(saturation current) J_L(light generated current) q (elemental charge) k_B(Boltzmann constant) T (temperature in Kelvin) A (ideality factor) R_s(series resistance) R_{sh}(shunt resistance) η (power conversion efficiency) The standard input power is 100 W/cm^2
Eq.5	$\boldsymbol{FF} = (V_{mp} * J_{mp})/(V_{oc} * J_{sc})$	
Eq.6	$J = J_0(\exp(q(V - JR_s)/(Ak_BT) - 1) + (V - JR_s)/R_{sh} - J_L$	
Eq.7	$\boldsymbol{V_{oc}} = Ak_BT/q * \ln(J_L/J_0 + 1)$	
Eq.8	$\boldsymbol{\eta} = V_{oc} * J_{sc} * FF/Input\ power$	

4.2 Quantum Efficiency (QE)

To further understand the photo conversion process, external quantum efficiency (EQE) measurements can be performed on the complete solar cell. EQE is defined as the ratio of the number of the collected carriers from the

[8] The reasons are still under debate. It has been shown that either an electron barrier on buffer/absorber interface or a hole barrier at the absorber/back contact can contribute to the crossover behavior of the J-V curves.

incident number of photons of a given wavelength into the solar cell. In other words, it can be regarded as the convolution of the generation profile of electron-hole pairs in the solar cell and the collection efficiency of these carriers that contributes to the external current. This means by incorporating the photon flux of the AM1.5 solar spectrum ($\Phi_{AM1.5}(\lambda)$), the photocurrent can be calculated from the EQE setup (see Eq. 9). The calculated J_L from EQE is often used to correct the J_{sc} derived from J-V characteristics.

$$J_L = q\int_0^\infty \Phi_{AM1.5}(\lambda)EQE(\lambda)d\lambda \quad \text{(Eq.9)}$$

EQE is useful for analysis of thin film solar cells, as carrier loss mechanisms sometimes may be indicated by the shape of the EQE curve. *Figure 8a* presents the EQE of a typical CIGS thin film solar cell that is analogous to CZTS. Five carrier loss paths that limit reaching the theoretical current density of this CIGS solar cell (a bandgap energy of 1.13 eV) are marked, and the resulting current loss from each path is summarized in *Figure 8b*. Except for region (5), i.e. current loss in relation to imperfect CIGS film, all rest of the current loss paths are related to non-optimal optical management of the entire CIGS solar cell stack. In (5), the current loss due to the incomplete absorption is an issue only for ultra-thin films (< about 1 μm). To take a closer look at electrical losses for the solar cell, internal quantum efficiency (IQE), that only considers the absorbed incident photons of a given wavelength, is required. An IQE curve can be derived from EQE by extracting the reflectance and transmission of the solar cell. It can be approximated by,

$$IQE = 1 - \exp(-\alpha(\lambda) * w(V))/(\alpha(\lambda) * L_e + 1) \quad \text{(Eq.10)}$$

Where $\alpha(\lambda)$ is the absorption coefficient of the absorber material, $w(V)$ is the width of space charge region and L_e is the electron diffusion length. By applying bias voltage or performing numerical simulation, all variables in Eq.7 can be potentially derived and be used to compare with results from other device characterization techniques such as electron beam induced current and capacitance-voltage measurement [88-92].

QE can also reflect the bandgap energy of the absorber material. This is done by evaluating the QE edge in the long wavelength regime since this relates to the optical absorption edge. *Figure 8c* displays three main methods, which are widely presented in literature, to derive bandgap energy from the QE edge. In CZTS, values from these methods often diverge, which indicates that CZTS quality is inferior. Unlike a perfect material, defects in a material often introduce band tails (Urbach tails) that locally narrow the band edges, leading to the QE edge changing from an ideal abrupt to a sloped shape. As shown in *Figure 8a*, region (6) could be a result of the collected carriers that are generated from band tail states. The band tail can contribute to the J_{sc} of a

solar cell but can also lead to a decrease in V_{oc}. As discussed in section 3.3, the band tail could stem from a high defect density such as Cu/Zn cation disorder. The Cu/Zn order-disorder transition has been demonstrated to relate to the shift of QE edge, which could yield an improvement of V_{oc} but unchanged overall device performance [78, 93].

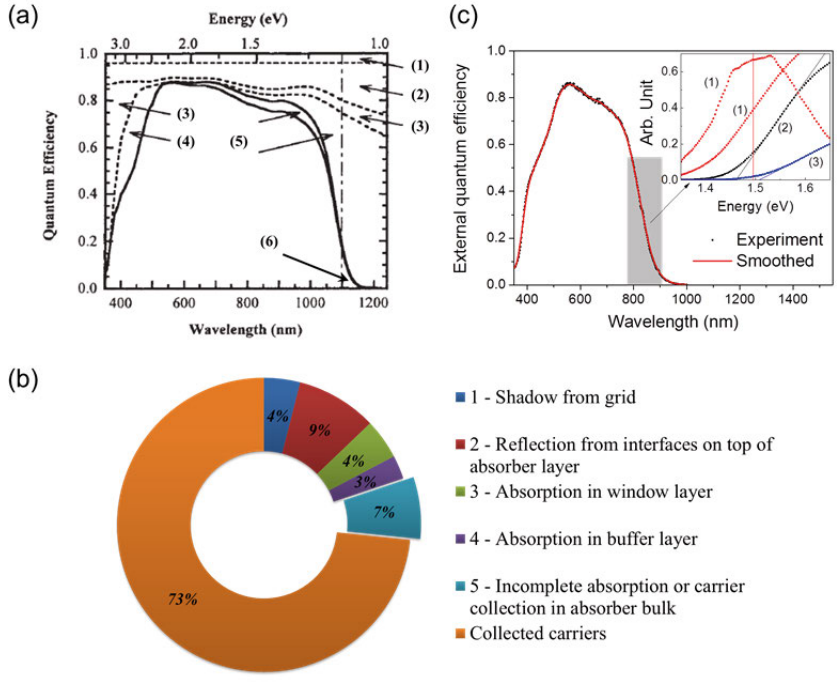

*Figure 8. (a) External quantum efficiency of a typical CIGS thin film solar cell: (bottom solid curve), 0 V; (upper solid curve), -1 V. The graph is reproduced from [89]. The dot dash line marks the estimated bandgap of CIGS material. (b) Percentage of current loss from the ideal 42.8 mA/cm^2 due to different process indicated in (a); (c) EQE of a CZTS solar cell, the inset shows various methods to determine E_g from the EQE edge at near IR regime (gray area). In the case of shown sample, E_g value are (1) 1.50 eV, First derivative of normal EQE curve (2) 1.51 eV, E vs (E*ln(1-EQE))^2 (3) 1.46 eV, E vs EQE^2.*

5. Fabrication of CZTS Solar Cells

5.1 CZTS Precursor Deposition

To prepare CZTS absorber layers, a two-step process was conducted throughout the thesis work. At Ångström Solar Center (ÅSC), this includes co-sputtering at low temperature in the first step and a high temperature thermal process in the second. To ensure proper sulfur incorporation into the CZTS precursor film, either reactive co-sputtering of compound and metallic targets or co-sputtering of compound targets was performed.

5.1.1 Reactive Co-sputtering of Cu_xS, Zn and Sn Targets

The reactive (co-)sputtering process was conducted in a Von Ardenne CS600 sputtering system, as outlined in *Figure 9*. The system was configured with three magnetrons facing the substrate with an angle of 45° at a distance of 16cm. 4-inch planar circular targets of Cu_2S or CuS (purity 99.95%), Zn (99.99%) and Sn (99.99%) were used. All the targets were operated in pulsed direct current (DC) mode. For Zn and Sn targets, pulsed DC with a frequency of 20 kHz was supplied by two Huttinger PFG 3000 DC power supplies, which were equipped with Advanced Energy Sparc-le 20 pulsing units. As to Cu_2S or CuS target, an Advanced Energy pinnacle® plus+ 5 kW pulsed DC power supply was connected and the pulsing frequency was set to 150 kHz. Constant power mode was applied to yield the desired power density on the respective targets, thereby targeting a particular cation composition of the final precursor film. The base pressure of the system was below 10^{-6} Torr. The standard process pressure was 5 mTorr with either mixed 1:1 H_2S (99.5%) /Ar or full H_2S (99.5%) constant flow at 30 sccm. The substrate holder was intentionally heated up to 180 °C in order to adjust the stress in the precursor film, and 7 pieces of identical precursors could be produced in one sputtering batch. Since there is a linear relationship between film thickness and (X-ray fluorescence) XRF counts, we can simply modify the deposition rate by examining XRF counts. A typical sputtering time of 20-60 min can produce a 500-1500 nm thick CZTS precursor.

Precursors prepared from the reactive sputtering process were used for papers I-III, IV and VI. The baseline precursor at ÅSC has cation composition

of Cu-poor, Zn-rich, Sn-rich precursors (Cu/Sn < 2, and Zn/(Cu+Sn) > 0.33), and a thickness of about 800-1000 nm according to the study in paper II.

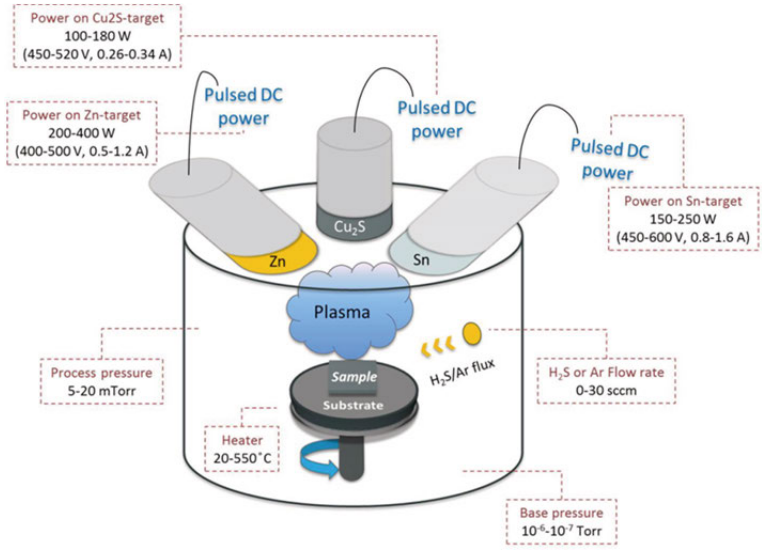

Figure 9. Schematic of reactive co-sputtering process performed in this thesis work

5.1.2 Co-sputtering of CuS, ZnS and SnS Targets

The key issue using the reactive co-sputtering process at ÅSC is the instability of the Zn target and resulting Zn incorporation into precursor films. The exact reasons are still uncertain during the period of this thesis work: it could be related to uncertain growth rate of a ZnS insulating layer on the surface of Zn target, or Zn sticking property on the deposited film. Therefore, CZTS precursors were also prepared from co-sputtering of compound targets.

The co-sputtering process was conducted in a Kurt J. Lesker sputtering system configured with 3-inch planar circular CuS, ZnS and SnS compound targets. TruPlasma DC 4002 power supplies were operated on the CuS and SnS targets, while a Kurt. J. Lesker Company radio frequency (RF) power unit was connected to the ZnS target. Constant power mode was applied to all targets for tuning the deposition rate and thus the composition of the deposited film. The base pressure of the system was below 10^{-6} Torr. The sputtering pressure was 5 mTorr at a constant Ar flow of 50 sccm. The substrate holder temperature was kept at 250 °C, and a typical sputtering time of 50 min produces around 1000 nm thick CZTS precursors. Eight pieces of identical samples can be produced in one sputtering batch. Precursors produced from the compound co-sputtering process were used in papers V and VII.

5.2 CZTS Absorbers

The high temperature (> 550 °C) annealing process following the sputtering process is a crucial step to improve the quality of CZTS films. Since kesterite material tends to decompose due to the difficulty to control the P_{S2} at high temperature, a graphite box with limited volume is usually utilized for this process, given that the gas/vapor pressure for a fixed loading of solid chalcogen is inversely proportional to the volume of the closed system at a constant temperature.

Figure 10 shows the setup of the home-made tube furnace for annealing CZTS precursors in this thesis work. It consists of four zones:

1. Loadlock, Zone 4, to load and unload the samples by pumping/purging N_2 gas;

2. Transition zone, Zone 3 that is close to the gate valve between Loadlock and cooling zone, to rest the samples before/after annealing process;

3. Cooling zone, Zone 2 that is configured with a water-cooled Cu coil, to enable a fast cooling after completion of the annealing.;

4. Hot zone, Zone 1 that contains a graphite block to receive the samples, and is heated by electrical resistance, to perform the main part of the annealing process;

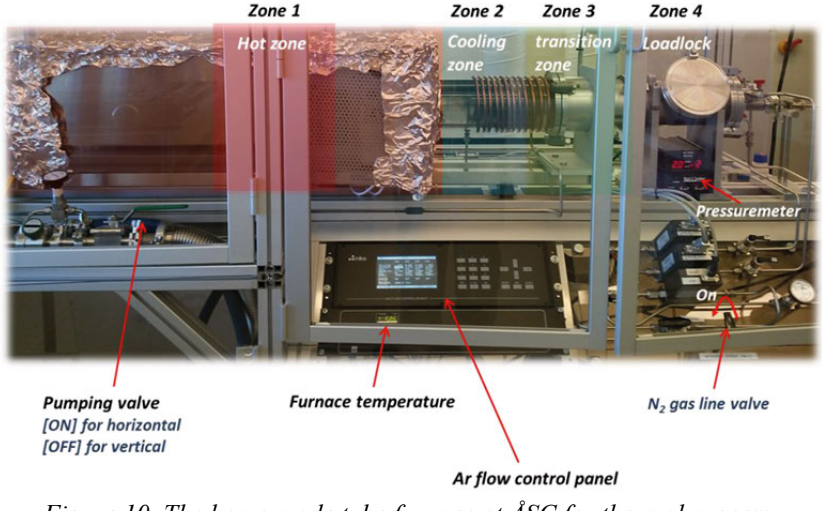

Figure 10. The home-made tube furnace at ÅSC for thermal process

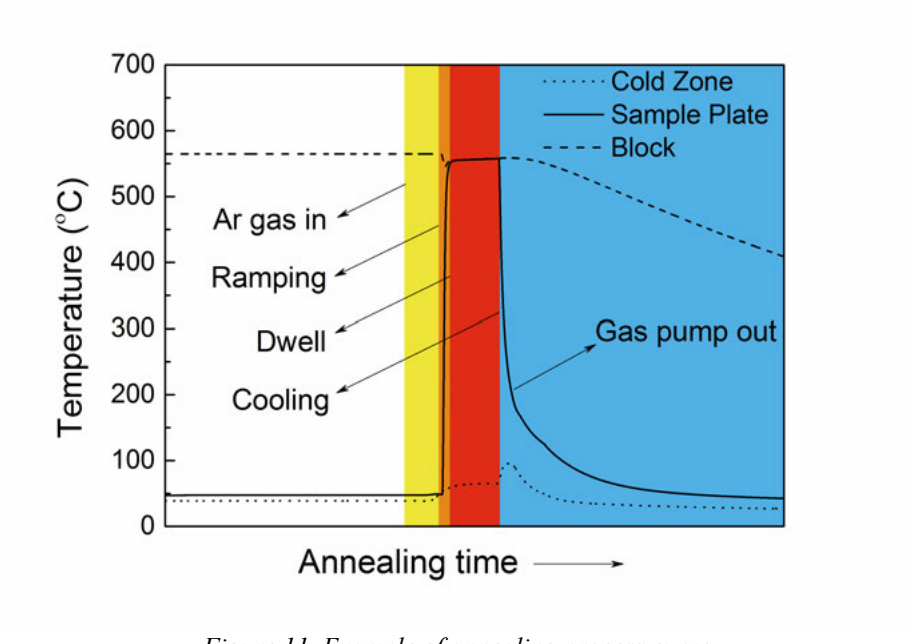

Figure 11. Example of annealing process curve

In order to achieve a rapid thermal process with a high ramping rate, the hot zone is usually preheated to the set temperature, and once the temperature of the block is stabilized, the CZTS precursors will be loaded in the furnace ready for the annealing process. The fast ramping is realized by inserting the sample plate to the hot zone from the transition zone. The sample temperature during the annealing process is recorded by a thermocouple embedded into the titanium sample plate. An exemplary process curve is outlined in *Figure 11*. When the block temperature is stabilized at the set temperature, Ar gas is firstly purged into the furnace until the total pressure reaches 260-350 mbar. The sample plate is then immediately inserted into the hot zone after the Ar pressure valve is closed. After completing the annealing dwell, the sample plate is quickly withdrawn to the cold zone for cooling to below 50°C. Herein, all gases inside the furnace will be pumped out after the sample plate is cooled to 200 °C. The average ramping and cooling rates are generally about 5.5 K/s and 0.2 K/s, respectively. Maximally four precursor films (each size of 2.5x2.5 cm^2) can be loaded into a 5x5 cm^2 pyrolytic-coated graphite box. To enable a saturation vapor pressure of chalcogen species over the CZTS sample surface in the graphite box, an excess amount of solid sulfur is always loaded. Differences in preparation of the CZTS absorbers in different papers are summarized in *Table 4*.

Table 4. Summary of the treatments of precursor films performed in this thesis work

Papers	Precursor	Annealing in S atmosphere	Annealing in Se atmosphere	Ordering process	Post annealing
I-III, IV and VI	Reactive (co)-sputtered	560 °C, 10 min, 265 mbar Ar			
V	Co-sputtered	580 °C, 0-40 min, 350 mbar Ar		Re-heat to 300 °C, and then cool down with 0.1 K/s to 80 °C under 300 mbar Ar	
VII	Co-sputtered	580 °C, 13 min, 350 mbar Ar	560°C, 4min, 265mbar Ar		10 min in Air, 100-300 °C on hotplate

5.3 Fabrication of CZTS Solar Cells

The baseline process for device fabrication in this thesis is described in *Figure 12*. Initially, about 350 nm Mo is DC-sputtered on the cleaned 1mm thick SLG of size 10x10 cm^2. The Mo coated SLG substrates are then cut into pieces of 2.5x2.5 cm^2 for CZTS deposition. After finishing the thermal process to convert CZTS precursor into active CZTS absorber, the samples are etched in 5 wt% KCN solution for 2 min, in order to remove unfavorable surface compounds like Na_2S (Paper VI) [45]. Following the etching process, about 50 nm thick CBD-CdS buffer layer is deposited on the cleaned CZTS absorber surface. The chemical solution is mixed with 0.005 M cadmium acetate, 0.07 M Thiourea and 1.14 M Ammonia. The water bath temperature is pre-heated to 60 °C. The samples are immersed into the chemical solution at room temperature before the reaction beaker is moved to the water bath. The timer starts as soon as the beaker is placed into the hot water bath. When the CdS layer deposition is completed, the samples are rinsed in two batches of deionized water successively and then flushed under the water tap. After drying with N_2 gun, the CdS deposited CZTS samples are immediately moved to the Von Ardenne sputtering system for RF sputtering of window layers. The window layer is composed of about 80 nm sputtered i-ZnO layer followed by 210 nm AZO layer. Finally Ni/Al/Ni contacts are evaporated onto the Al doped ZnO layer. Ni layers are used to prevent Al from formation of the resistive Al_2O_3, since Al can react with oxygen that is from either the window layer or the air. For JV measurement, solar cells of 0.5 cm^2 total area are defined by mechanical scribing.

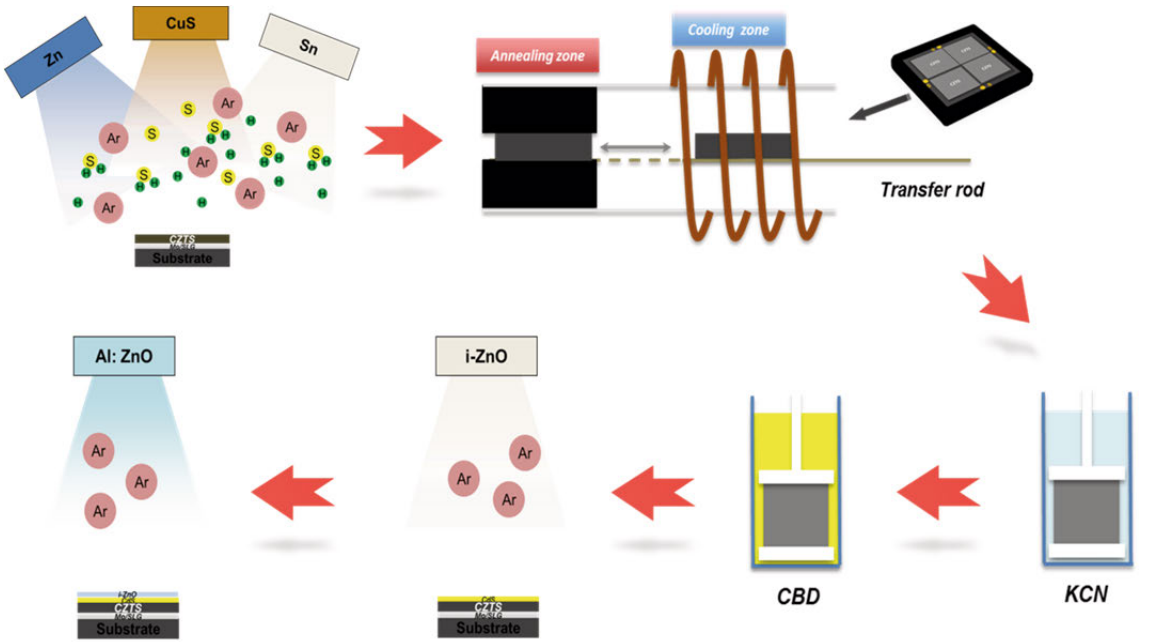

Figure 12. Process flow of CZTS solar cell fabrication at ÅSC at Uppsala University

6. Material and Device Characterization Techniques

The material characterizations provide means to understand fundamental properties of materials or to monitor the process for material synthesis. In case of CZTS, due to the complexity of the material properties, complementary material characterization techniques are often required. The majority of the techniques performed in this thesis work will be introduced in this section.

6.1 X-ray Techniques

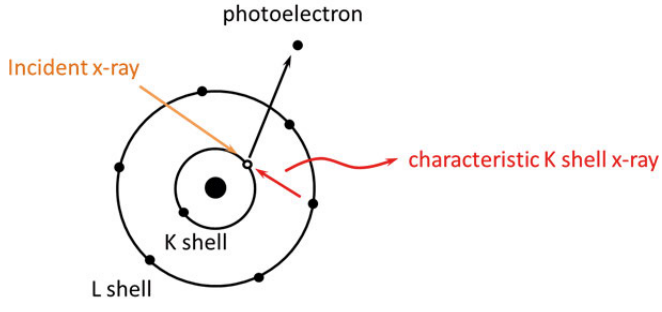

Figure 13. A schematic of principle of x-ray techniques; the photoelectron can be used for the XPS measurement, while the characteristic x-ray can be used for the chemical quantification.

X-ray based technology is widely used to identify phases or compounds, to analyze their crystal structure and to determine their chemical composition. As shown in *Figure 13*, the photon energy provided by an incoming monochromatic x-ray beam can excite an electron to vacuum from the K shell of the atom, and the ejected energetic photoelectron can be used for x-ray photoelectron spectroscopy by measuring its kinetic energy. Simultaneously, an electron from L shell can relax down to the ground state to re-emit a specific x-ray energy that is characteristic of the element concerned – this "X-ray fluorescence" can be used to quantify the elements in a sample.

X-ray fluorescence (XRF)

XRF is used to determine the chemical composition of CZTS thin films. At ÅSC, the XRF measurement is calibrated by the Rutherford backscattering spectroscopy, as described in detail in [94]. XRF measurement is conducted in a PANalytical Epsilon 5 system. The measured spot size on the sample is about 2cm in diameter. Two important remarks need to be stressed for this measurement on CZTS: 1) the cation composition calculated from XRF is an average value, since the typical CZTS sample has the size of 2.5x2.5cm^2. 2) Because Mo substrate is used for CZTS thin film deposition, XRF cannot be used to derive the anion composition of CZTS thin film due to the overlap of the energy of S-K and Mo-L. The accuracy of the XRF composition is about 0.5-2at%, depending on the element as well as the film thickness. XRF measurement was used in all papers.

X-ray photoelectron spectroscopy (XPS)

XPS is a surface sensitive technique (usually few nanometers in depth from the material surface) that allows identifying chemical environment of the CZTS surface. As displayed in *Figure 13*, the binding energy can be calculated by subtracting the work function and the kinetic energy of the ejected photoelectrons from the incident x-ray energy. By comparing experimental results to reference data, the compound can be recognized. In order to cross-compare XPS results among different samples, one should pay close attention to the carbon contamination or oxidation on the surface of the samples. In paper VI and VII, XPS was performed to identify Na related compounds as well as to compare surface properties of the oxidized CZTSSe thin films before and after etching process. The measurement was conducted in a PHI Quantum system with monochromatic Al-Kα x-ray source. The measurement spot size is 200μm.

6.2 X-ray Diffraction (XRD)

XRD is a technique used to characterize the crystal structure of materials. An incident monochromatic x-ray beam (a Cu Kα radiation (λ=0.15406 nm) source) is elastically scattered after striking atomic planes with spacing d. If the reflected x-ray from the crystal for a given angle between the source and detector has a light path fulfilling the Bragg law, they will constructively interfere and a signal will be detected. In a standard Bragg-Brentano setup, the angle of the incident beam towards the normal of the material surface is identical to the angle of the outgoing x-ray towards the detector, namely θ-2θ configuration. To assign the diffraction pattern to the crystal structure of

any material, one should always compare experimental data to reference data such as PDF cards or ICDD database. Nonetheless, materials prepared for the reference data are often in powder form, making it difficult to fully apply to thin films. This is because thin films have much less material mass (so smaller signal), and are susceptible to preferential orientation or strain.

Fortunately, grazing incidence XRD (GIXRD) techniques can resolve the issue of low signal of the grown thin film. In GIXRD setup, the angle of the incidence beam is fixed while the detector is the only movable unit. This setup allows an increase of the scattering volume in the investigated thin film that greatly enhances the x-ray intensity. However, one should note when analyzing GIXRD of the thin film that may contain preferential orientation of the grain ensembles. For example, it works fine for the symmetrical scan of θ-2θ XRD to detect the grain orientation that has its normal perpendicular to the film surface, but this lattice plane cannot be detected by GIXRD due to the asymmetrical setup of GIXRD. This effect has been seen in identification of SnS phase with [004] orientated orthorhombic structure on the backside of CZTS thin film (Paper II, III, V).

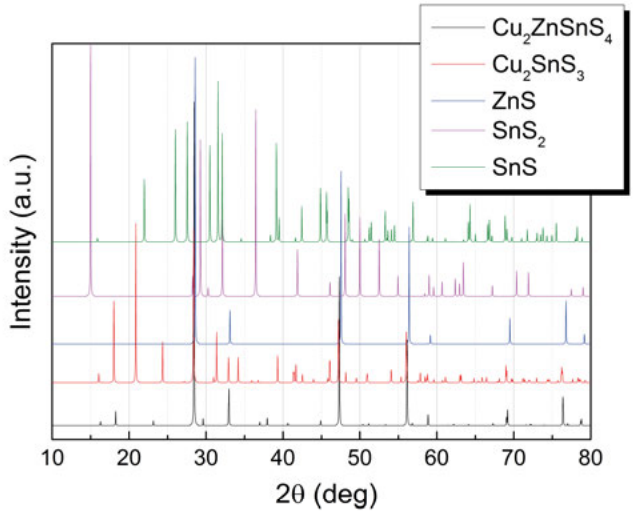

Figure 14. Example of XRD pattern of different phases in CZTS system; All patterns are simulated by PowderCell software and the data are from PDF cards: CZTS (#015-0223), CTS (#010-5719), ZnS (#005-0566), SnS_2 (#023-0677) and SnS (#075-0925)

In CZTS, the utilization of XRD technique has limitations. The major problem is the difficulty to separate cubic-ZnS, cubic-Cu_xS, tetragonal-Cu_2SnS_3 and tetragonal-CZTS phases in CZTS thin film due to the similarity of their crystal structures. *Figure 14* shows some simulated XRD pattern of possible phases in the CZTS system. It can be found that XRD is sufficient to identify

Sn-based secondary phases in CZTS, but that it is impossible to distinguish the cubic ZnS phase. A method like Raman scattering should be performed in order to complement XRD techniques for a better understanding of the material properties in CZTS. In this thesis work, XRD was performed in Siemens D5000 system, and GIXRD was conducted at 0.5-1.5° incidence angle in parallel beam geometry.

6.3 Electron Microscopy Characterization

Electron microscopy is among the most widely used techniques to picture the morphology of synthesized materials as well as their chemical composition. The core character of this technique lies in the control of interaction volume as displayed in *Figure 15*. The incident electrons penetrate into the material surface via elastic and inelastic scattering. The interaction volume has a pear-like shape into the material from the probe area, as sketched by the black curve in *Figure 15*, and its dimension depends on the primary beam energy, material density and atomic number of the material. The secondary electrons scattered close to the surface of the sample are collected to image the morphology of the material (SEM). The backscattered electrons are elastically scattered due to the repulsion of the atom nucleus, and have high energy. The non-escaped electrons will continue to interact with the material, leading to characteristic and continuum x-rays emitted from the bulk of the interaction volume. The characteristic x-ray can be collected for chemical composition measurement (EDS).

Scanning electron microscopy (SEM)

SEM can provide quite good spatial resolution within nanometer scale. Reducing the accelerating voltage is a way to improve the resolution for a better imaging of surface topography. However, too low accelerating voltage can result in false image of the material due to the surface contamination from the absorbed carbon from the environment in the chamber. In contrast, using too high accelerating voltage can lead to losses of morphological information of the material surface, but may help to investigate alternative information deeper into material. Since the SEM image is produced by collecting secondary electrons, which means materials with low conductivity can introduce charging effect thus influence the image quality. In the case of CZTS film, this could be used to distinguish CZTS grains and ZnS crystals (usually bright), since ZnS is an insulator.

In this thesis work, a Zeiss Leo 1550 with Gemini electron column and in-lens detector was used. The accelerating voltage of was typically set to 5 kV for SEM images.

Energy dispersive x-ray spectroscopy (EDS)

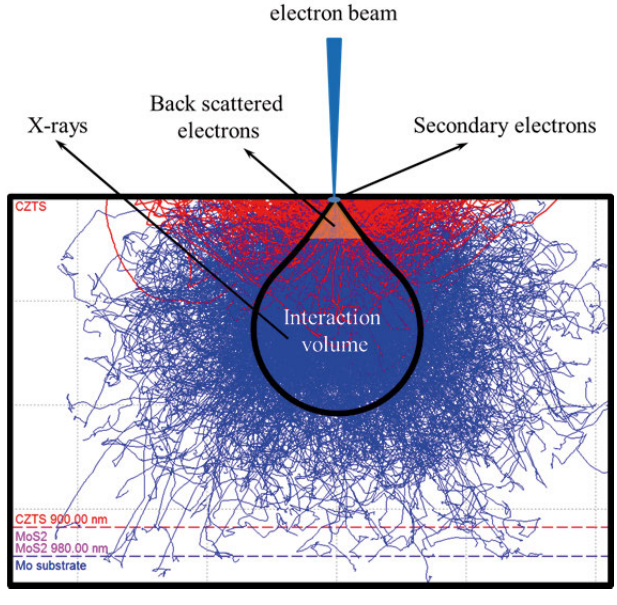

Figure 15. Monte-Carlo simulation of the Interaction volume induced by the primary electron beam energy at 12 keV; the analyzed CZTS thickness is 900nm; the red color reflects the back scattered electrons. The electron energy is faded as the density of the electron trajectories (blue color) inside CZTS becomes less. The secondary electrons ejected near the probe surface are used for SEM image, while the emitted characteristic x-ray from the bulk material is used for EDS quantification.

As a module attached to the SEM system, EDS enables a direct quantification of the chemical composition in the area of interest during the investigation of the material morphology. Similar to XRF, EDS is not reliable for Mo and S measurement due to their energy overlap. Yet differing from XRF, the spatial resolution of the EDS measurement is on the scale of a few hundred of nm to mm. However, the resolution is strongly dependent on the interaction volume shown in *Figure 15*. This means that morphological effects can greatly influence the EDS result. In addition, the EDS software generally considers that the material is uniformly mixed, which can possibly lead to incorrect analysis of thin film materials, particularly for films with layered structures. The accuracy of the EDS measurement is about 2-3 at%, depending on the quality of material, elements of interest, conditions of the measurement and the analysis software. Therefore, one should take precautions

when making conclusions on basis of the quantification of the chemical composition derived from EDS data. Despite these shortcomings, EDS is still powerful for qualitative compositional mappings with proper measurement settings.

In this thesis work, an Oxford instruments EDS system was used. The accelerating voltage was varied from 5-20 kV depending on the characterized material. The compositional analysis is resolved via Oxford Instruments software Aztec.

Electron beam induced current measurement (EBIC)

EBIC is another measurement that can be carried out in a suitably equipped SEM system, which allows measurement of electrical properties on solar cell devices, in particular of carrier collection. Instead of using a light source, the incoming electron beam from the filament of the SEM generates electron-hole pairs inside the solar cell. An external EBIC current can be measured when the generated carriers are collected. The EBIC current depends on the electron beam energy and current, the material properties, electrical properties of the solar cell, and the position of the irradiation. In other words, the EBIC current is the convolution of the generation and the collection functions of the electrons in the solar cell. If the electron-hole pairs are generated in the proximity of the pn junction, the probability of their collection gets higher. EBIC can be used to extract the electron diffusion length by means of numerical and analytical simulations [95]. EBIC measurements can be performed in both top-view and cross-section configurations.

Despite the advantages of EBIC measurement, one should also be cautious of its critical issues. EBIC results can be greatly affected by the morphology and surface states of the sample. This is particularly a problem for cross-section EBIC. The macro-scale roughness of the surface is commonly seen after breaking samples for cross-sections. Besides, the new surface of the cross-section can introduce surface states to enhance the surface recombination, which makes the measurement with small accelerating voltage unreliable. Nevertheless, by depositing a passivation layer on cross section surface [96] or comparing to top-view EBIC on the same sample, one can partly resolve this issue. *Figure 16* shows an example of EBIC and its comparison to a SEM image. It is notable that by comparing top-view as well as cross sectional EBIC and SEM at the same time, the sample morphology and electrical properties as well as their correlation can be observed. The measurement can be more complete with the combination of chemical mapping by EDS in the same SEM setup.

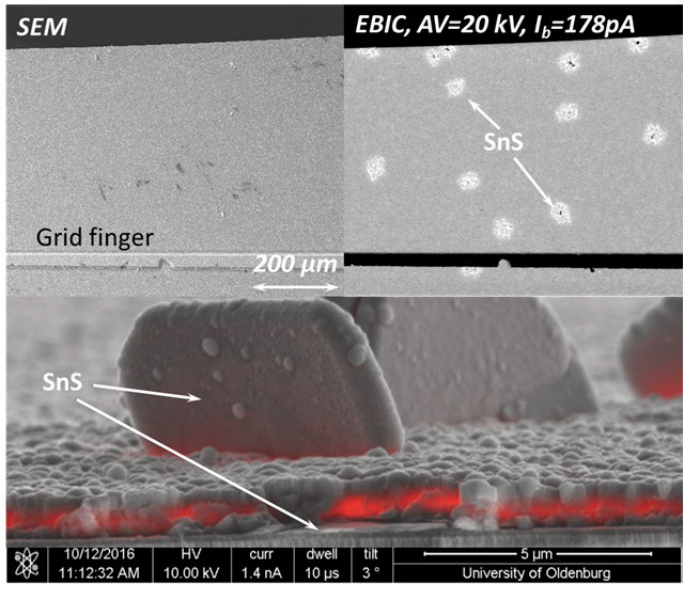

Figure 16. SEM and EBIC of thin CZTS solar cells (upper figures) Top-view comparison; (bottom figure) the overlayed cross section SEM and EBIC images (red)

In paper III, EBIC at Oldenburg University, Helmholtz Zentrum Berlin and Uppsala University were tested on sister CZTS solar cells. In Uppsala, EBIC was carried out by connecting an AMETEK Model 181 low-noise current preamplifier to existing SEM detector input channels.

6.4 Optical Characterization

Raman Spectroscopy

Raman spectroscopy is a powerful tool to characterize material crystal structure and quality of the material, and it is a useful complementary technique to other techniques such as XRD. The Raman effect originates from the polarization of the dipoles in solids when an incoming laser beam interacts with the phonons of the probed material. The resulting elastic light scattering is regarded as Rayleigh scattering, while the inelastic scattering with reduced energy is referred to as Stokes Raman scattering (the reverse process is called anti-Stokes Raman scattering). Furthermore, when the performed excitation laser wavelength approaches the electronic bandgap of the semiconductor material, certain chemical bonds in material can be greatly disturbed, yielding much stronger Raman signals for some vibrational modes, namely (near) resonance enhanced Raman scattering (NR-Raman).

One of the advantages of using Raman for CZTS is to identify phases. This procedure is usually done by comparing experimental spectra to the data from reference material. Examples for CZTS thin films are suggested in *Figure 17*. By performing multi-wavelength Raman and comparing to reference material, various secondary phases can be identified. The main vibrational modes of these secondary phases of CZTS, which are sensitive to particular laser wavelengths during Raman measurement, are summarized in *Table 5*.

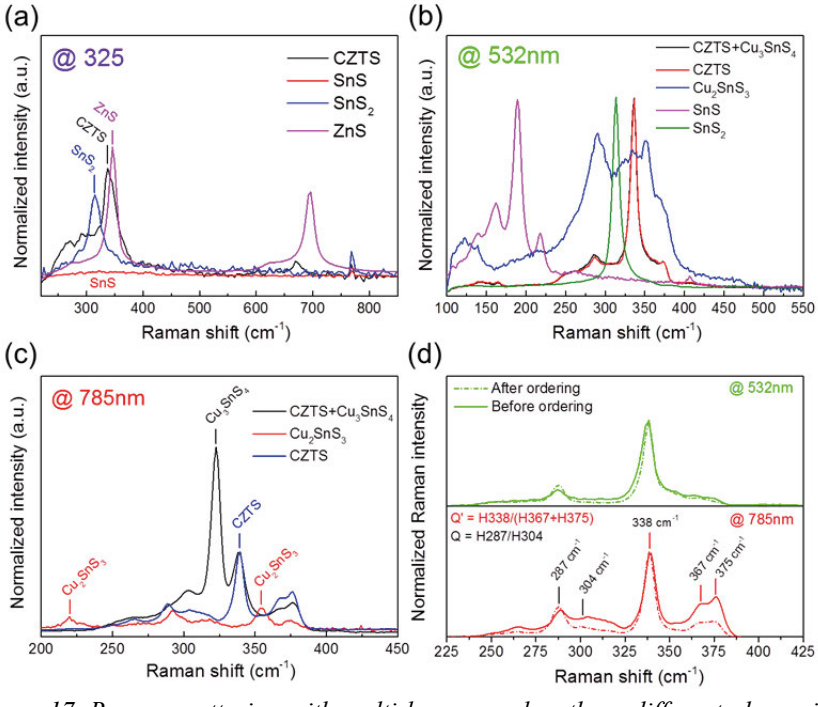

Figure 17. Raman scattering with multi-laser wavelength on different phases inside CZTS film: (a) UV laser; (b) green laser; (c) near infrared laser; (d) Raman scattering of the CZTS samples that were treated with/without ordering process.

Another advantage of using Raman is to study defects in the CZTS phase (at least those that occur at high enough concentrations to perturb the lattice phonons), in particular cation disorder. The Cu/Zn cation disorder (Cu_{Zn}+Zn_{Cu} defect pair) has a high concentration, due to the similarity of the Cu^{+} and Zn^{2+} cation size and its low formation energy [10, 11]. The order-disorder transition results in a change in the concentration of this defect pair which is visible as peak intensity change in the NR-Raman (see *Figure 17d*), and the transition temperature of about 265 °C has been determined [15]. In *Figure 17d*, it is noticeable that the reduction of the Cu-Zn disorder drastically improves the overall structural quality of CZTS film, when a low tem-

perature ordering process [15] or an optimized cooling process was adopted after the main annealing process [16].

Table 5. Summary of phases in CZTS film that can be measured by Raman of different laser wavelength. The wavenumber in the bracket represents the most characteristic Raman peak.

Excitation wavelength	Most sensitive phases	Reference
325nm	ZnS(346cm^{-1}), SnS_2(315 cm^{-1})	Paper V, [97]
532nm	CZTS(338 cm^{-1}), SnS_2(315 cm^{-1}), Sn_2S_3(308 cm^{-1}), SnS(190 cm^{-1}), Cu_2SnS_3(293 cm^{-1} and 353 cm^{-1})	Paper V, [20, 98, 99]
785nm	CZTS(338 cm^{-1}), Cu_3SnS_4(321 cm^{-1})	[98, 100]

The main drawback of using Raman scattering for CZTS is the limited depth resolution. The light penetration for a given laser wavelength is inversely proportional to the absorption coefficient of the investigated material at that wavelength. For standard 1000 nm thick CZTS films, this means only about 200 nm (near infrared laser) from the material surface can be measured. In this thesis work, micro-Raman measurement at room temperature and ambient air were performed in a Renishaw inVia system, and the laser wavelengths of 325 nm, 532 nm and 785 nm were typically used. The laser power was generally below 0.3 mW, and the spot size of the laser on sample surface is about 1-5 μm depending on the laser wavelength and numerical aperture of the objective. Treatment of Raman data is done by using the Wire3.4 software. Discussion on Raman results is shown in Papers I, II, III, V and VII.

Photoluminescence (PL)

PL measures the energy emitted from the recombination of electron-hole pairs that are initially generated by absorbing an incident laser wavelength, and thereby is widely used to study defects in semiconductor materials. However, only radiative recombination process are measureable by PL. At room temperature, only band-to-band transitions are normally visible, but in CZTS, tail-to-tail or band-to-tail transitions are dominant due (in part) to the Cu/Zn cation disorder, which can lead to bandgap fluctuations and overall bandgap narrowing of upto 200 meV from its ideal 1.5 eV [77]. Thus, PL peak for CZTS is usually below the bulk bandgap. In this thesis work, PL at room temperature was performed in a Renishaw inVia system. Since interference effects are strong in thin film materials with large band tails such as CZTS and the prepared thin film is less rough, the PL is usually corrected with a calculated fringe pattern [101].

6.5 Solar Cell Characterization

Current-Voltage Characterization

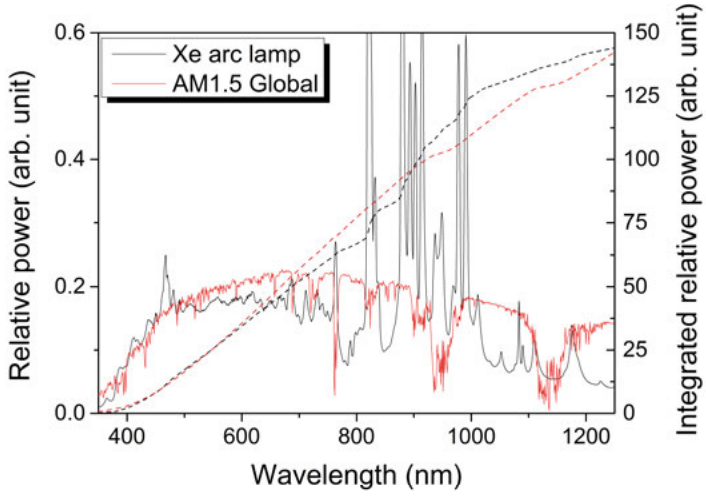

Figure 18. Comparison of the photon flux from AM1.5G solar spectrum and Xe arc lamp used for JV measurement in our lab. All spectra are rescaled for comparison, and the dash line shows the integrated result.

In this thesis, a Newport (class ABA) one-sun-illumination simulator was used to test the solar cell performance. A Xe arc lamp with AM1.5 filter was used as the light source, with the spectral distribution shown in *Figure 18*. The light intensity for CZTS solar cells was calibrated by comparing to the J_{sc} derived from the QE measurement. As indicated by the integrated curve (dash line) in *Figure 18*, the adjusted power for the spectral intensity of the solar simulator matches well with the current from AM1.5G solar spectrum for a pure CZTS device. However, if keeping the same power, one may overestimate the current of the device that has a lower bandgap around 1.13-1.2 eV, such as for CZTSSe solar cells.

Quantum efficiency

A home-made QE setup was used for this thesis work. Extracting bandgap from QE edge was shown or discussed in papers II, IV, V and VII.

7. Results and Discussion

7.1 Formation and identification of equilibrium secondary phases using baseline annealing process (Paper I)

Reactively sputtered precursors could promote metastable phases because the sputtering deposition is a kinetically limited process in which the low adatom surface mobility is affected by the kinetic energy from the adatoms or substrate temperature. Since a high temperature step is necessary for CZTS formation, it is essential to understand the nature of the sputtered precursor and its conversion into an equilibrium state during annealing. This is also true for the secondary phases that are formed alongside the CZTS phase. To clarify the possible transitions of secondary phases from the metastable to the equilibrium condition, and identify their respective stable structures for our baseline annealing process, Cu–S, Zn–S, Sn–S, Zn–Sn–S, Cu–Sn–S and Cu–Zn–S films were prepared and compared. These films were then annealed in the same annealing batch.

Table 6. Summary of identified phases in the reactively sputtered films before and after the annealing process. ZnS indicates there may be a metastable ZnS phase. Reprinted from[20]. Copyright ©2017, with permission from Elsevier*

Sample	Phase assignment	
	Before annealing	After annealing
Cu-S	CuS	Cu_xS, MoS_y, ($1<x\leqslant 2$, $0<y\leqslant 2$)
Zn-S	ZnS	ZnS, MoS_y
Sn-S	SnS_2	SnS, MoS_y
Zn-Sn-S	Sn_2S_3, S, Zn_xSn_yS/ZnS* (x>0, y>0)	ZnS, SnS, MoS_y
Cu-Sn-S	Cu_2SnS_3	Cu_2SnS_3, $Cu_2Sn_{3.5}S_8$, MoS_y
Cu-Zn-S	Cu_xS, Cu_yZn_zS/ZnS* (y>0, z>0)	Cu_2ZnSnS_4, Cu_xS, ZnS, MoS_y

Table 1 summarizes the key results of Paper I. The phase assignment was obtained via combined characterizations of XRD, SEM-EDS and Raman scattering with two laser wavelengths (532 nm and 325 nm). It can be observed that unlike the Cu-Sn-S film, the Zn-Sn-S and Cu-Zn-S films do not form a uniformly alloyed phase during the reactive sputtering process. Since we cannot assign the Raman peak at 322 cm^{-1} (UV laser) or cannot separate

it from ZnS phase with confidence, it is speculated that this peak, which appears for the two ternary films, is also possibly belonging to a metastable feature of the reactively sputtered films. Upon annealing, the stable phases that are expected to exist under equilibrium were indeed formed. Nevertheless, interesting results were noted for Sn-S and Cu-Zn-S films. The SnS_2 phase in Sn-S precursor film decomposes to SnS by losing S(g), which strongly suggests that the annealing process is under deficient P_{S2}. SnS, due to its high vapor pressure, can enter into the annealing environment to react with other films, resulting in a formation of CZTS phase in the initially Sn-free Cu-Zn-S film. This clearly demonstrates that Cu_2ZnSnS_4 is the most favorable and stable phase in the Cu-Zn-Sn-S system. Throughout this work, we also confirmed that Raman with green laser wavelength is particularly sensitive to Sn-S secondary phases and Cu_xSnS_y phases, and the ZnS phase gives a strong response to the UV Raman. As to identification of the Cu_xS phase, XRD is more suitable than Raman measurement. The acquired Raman spectra were used as references to distinguish secondary phases in CZTS films in other projects (see Raman spectra in section 6.3).

7.2 Influence of CZTS absorber thickness on thin film solar cells (Paper II)

Absorber thickness is an important parameter for thin film solar cell design. Since CZTS has a direct bandgap and high-absorption coefficient [57], it is in principle possible to synthesize a thin absorber layer to reduce the material cost. The minimal CZTS absorber thickness is determined by the minimal light path according to absorption coefficient at a bandgap energy (L_{light}) or the smallest effective collection depth in CZTS ($L_{collect}$). Herein the effective collection depth is the depth from which the generated charge carriers can be collected, which combines the depletion width and the length of charge carrier collection in the quasi-neutral region which is determined by the electron diffusion length and the back contact recombination velocity (see e.g. *Figure 5*). The aim of Paper II is to estimate the influence of CZTS thickness on solar cell performance, under the condition that the composition of all CZTS films is consistent.

In Paper II, it has been shown that the composition of the annealed CZTS films with different thickness remained unchanged compared to their precursors. Moreover, the material quality of all the films is similar according to the material characterizations such as XRD, SEM and Raman. This is a good indication that we can consider the CZTS absorber thickness is the only variable in this study. *Figure 19a* presents the solar cell performance as a function of CZTS thickness, and it is notable that all parameters followed the

same trend, i.e. all parameters are increased and saturated when the absorber thickness is above 750 nm.

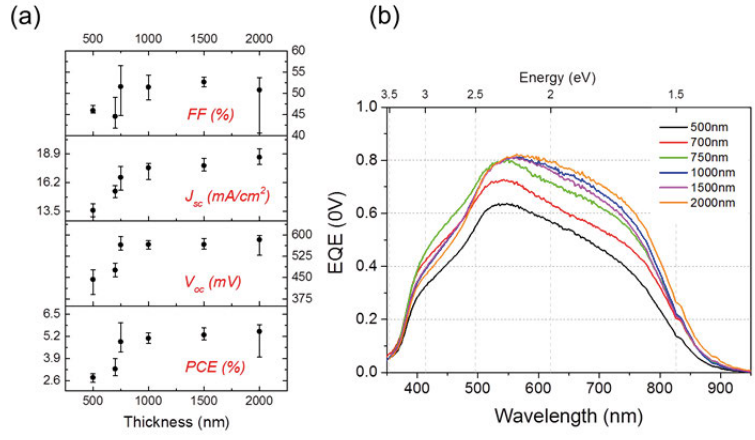

Figure 19. (a) Device performance as a function of CZTS absorber thickness; (b) EQE at 0V bias of the champion solar cell devices with the respective CZTS absorber thickness in (a).

The question raised here is which factor, i.e. L_{light} or $L_{collect}$, decides the minimal absorber thickness. Until now, there is scatter in literature reports about the exact absorption coefficient of CZTS [7, 57], and it is noticed from Beer Lambert's law in Paper II that the variation of absorption coefficient can influence the required absolute thickness of CZTS absorber. Since an expected enhanced EQE edge could be in relation to the improved absorption effect, we used EQE as a tool for this analysis. It is observed in *Figure 19b* that there was indeed a slight increase at the EQE edge with the increased CZTS thickness. Nevertheless, this effect, except for the 500nm thick film, smeared out when the reverse voltage biased EQE was performed (see Paper II). This reveals that the absorption is not a limiting factor for our CZTS film beyond 700nm thick, rather electrical loss is the issue. It needs to be stressed that the optical loss can still be a problem for solar cells with a CZTS film thickness smaller than 500 nm. Comparison of the (un-)biased EQE also implies that the effective collection depth of minority carrier in the CZTS absorber series is about 700-1000 nm. Poor device performance for thinner absorbers (500 nm and 700 nm) could arise from larger influence of lateral inhomogeneity, such as secondary phase segregation, or more generally to a reduced absorber quality at a level that is not apparent in material characterization, and enhancement of back contact recombination. *Figure 20* shows an EBIC measurement on the solar cell prepared from 2 μm thick CZTS. It is demonstrated that the effective collection depth starting from the surface of the CZTS film is indeed less than 1000 nm, which strongly supports the above discussion on basis of EQE.

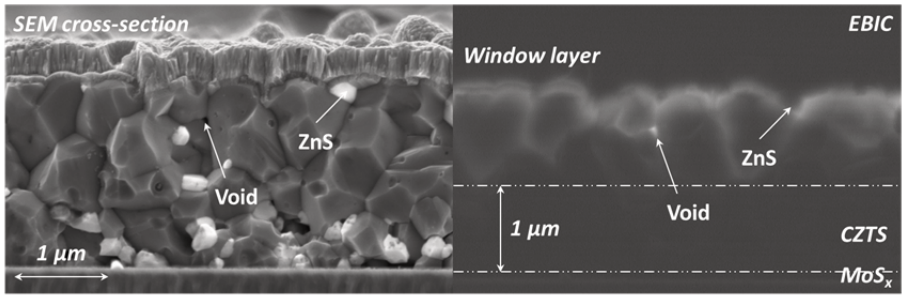

Figure 20. SEM cross-section and the corresponding EBIC of the solar cell prepared with 2µm thick CZTS film

In summary, it can be concluded that with the present CZTS material, no further gain would be expected for CZTS absorber thickness above 1000 nm. Thicker CZTS film becomes necessary only if the absorber quality can be continuously improved with an increased effective collection length of charge carriers.

7.3 Effects of secondary phases at the CZTS rear surface and an alternative rear passivation on thin film solar cells (Papers III and IV)

An import remark from the thickness study in section 7.2 is the identification of the ZnS and SnS secondary phases on both surface and backsides of CZTS film. The ZnS phase can also be identified in the CZTS bulk, as the bright particles indicated in *Figure 20* and by EDS mapping in *Figure 21e*. In contrast, the SnS phase cannot be observed in the CZTS bulk with the EDS mapping. The influence of ZnS on CZTS solar cells is briefly introduced in section 2.3.2. However, there is still a lack of understanding on the effect from SnS phases on CZTS thin film solar cells, which is the aim here.

In *Figure 21a-d*, it is notable that the SnS phase is apparently formed on both the surface and backside of the CZTS film in our standard annealing process. This phase seems to be highly orientated according to XRD in *Figure 21d*, and the intensive XRD peak at 31.8° suggests the SnS phase has orientation along the [001] direction with an orthorhombic structure. In fact, we can also observe that morphological orientation of the SnS phase in CZTS mostly occurs either perpendicular or parallel to the film surface, with a very flat plate shape, for example in *Figure 21e*. This is an evidence to support the preferential orientation of the SnS phase in our annealed CZTS film.

7.3.1 Investigation of effects of the SnS phase on CZTS solar cells via EBIC measurements

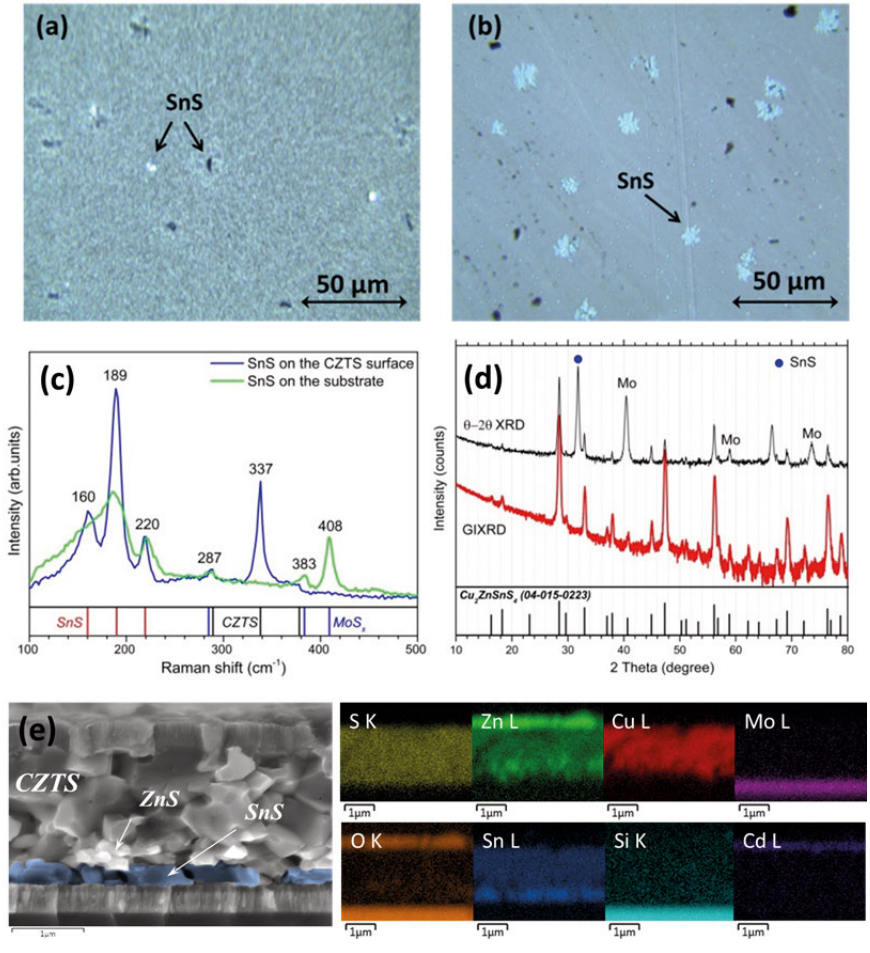

Figure 21. (a) Optical image of the film surface before and (b) after the annealed CZTS layer is mechanically lifted off (c) Raman scattering measured on the bright area present in (a) and (b); (d) θ–2θ and grazing incidence XRD of the annealed sample; (e) EDS mapping at 5keV on the cross section of CZTS thin film solar cell

Attempts to investigate the influence of SnS secondary phases on CZTS solar cells have previously used destructive methods such as etching CZTS film [59]. Here, we used EBIC measurements directly on CZTS solar cells to acquire an estimation of the impact of the SnS phases. The key results are presented in *Figure 22*. It is found that comparing to the average matrix of the CZTS film, the area covered by SnS on CZTS surface showed no EBIC signal, whereas the spots connected to the SnS phases on the CZTS rear displayed stronger EBIC signals. EBIC from both top-view and cross-section

configurations confirmed that the SnS phase on the CZTS rear improves the EBIC current by about 30% with respect to the areas without presence of any SnS phases. The reason for the positive effect of rear-contact SnS phase on the EBIC current may result from the passivation effect occurring at the CZTS/SnS rear interface. However, the formation of SnS phases may still result in local variations in CZTS material quality in terms of chemical composition which could counteract the beneficial effect from SnS phase at the CZTS rear. Therefore, to allow controlled CZTS/SnS interface, better CZTS bulk quality should be guaranteed.

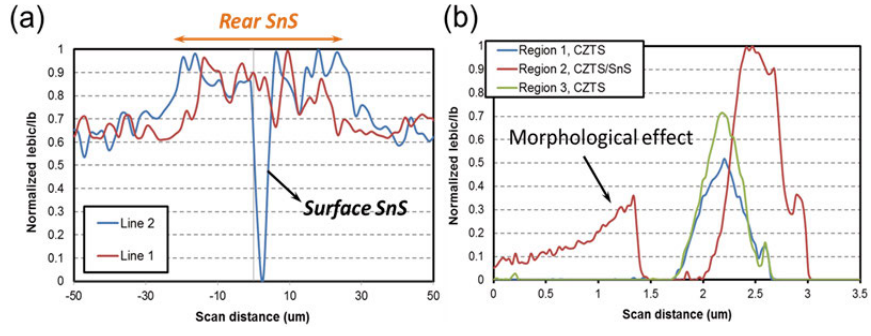

Figure 22. Extracted EBIC current from (a) top-view and (b) cross-section EBIC images in section 6.2

7.3.2 Passivation of CZTS rear contact with Al_2O_3 for ultra-thin solar cells

The passivation effect at the CZTS rear contact is expected to improve both V_{oc} and J_{sc} of the solar cell because the reduction in back contact recombination [102]. This effect can become apparent if the passivation area is large enough. For this purpose, deposition of a thin Al_2O_3 layer with nanosized-point-openings in between CZTS and Mo is attempted. An ultra-thin CZTS absorber of 400 nm was utilized for the comparison because the effective collection depth of the charge carriers in CZTS should be comparable to the absorber thickness to magnify the influence from the back contact, as was suggested by the thickness study (Paper II). In this work, NaF was supplied as a Na precursor source, since this treatment was demonstrated to be important for chalcogenide based solar cells [102].

In Paper IV, it was shown that the passivation layer of Al_2O_3 improves the V_{oc} of the final solar cells in general comparing to the reference CZTS solar cell without passivation layer. Taking a closer look at the EQE curves in Paper VII, it is noticeable that by comparing two device groups: i) reference and 1 µm pitch+5 nm NaF; ii) 2 µm pitch+5 nm NaF and 2 µm pitch+10 nm

NaF, the EQE starts to differentiate from wavelength larger than 550 nm and nearly converges into a similar ending. This indicates that the Al_2O_3 may enhance the CZTS device performance by either improving the back contact reflection or decreasing the back contact recombination velocity. The reason for the improvement of internal reflection may be due to the rougher Al_2O_3 layer seen in the TEM cross section. Nevertheless, the passivation effect is still not apparent for the Jsc enhancement. This could result from the still poor CZTS absorber bulk qualities, such as lateral structural inhomogeneity, that are paramount to improve. Additionally, it can be noted that after KCN etching of the annealed CZTS/ Al_2O_3/Mo film, the Al_2O_3 becomes rougher than the original neat layer. This may stem from the etching of Al_2O_3 layer in the KCN solution with strong basic environment, since Al_2O_3 is an amphoteric compound that is sensitive to basic solutions. Therefore, a process that employs Al_2O_3 to strive toward advancement of CZTS solar cells will require careful optimization.

In summary, the influence of the SnS secondary phase on CZTS thin film solar cells was characterized by EBIC measurements. It was found that this phase on CZTS rear can contribute to the current of the solar cell by means of a possible passivation effect. To further demonstrate the passivation effect, a thin Al_2O_3 layer with nanosized-opening was deposited on Mo/SLG substrates before the deposition of ultra-thin CZTS films. Although the V_{oc} of the solar cell can be slightly improved by this approach, the device still remains poor. The reasons are still open, but again it indicates that the bulk quality of the CZTS films must be improved.

7.4 Monitoring of sulfur partial pressure (P_{S2}) during the annealing process (Paper V)

Among the key issues for synthesizing CZTS material is to precisely control P_{S2}, in particular the chemical instability of CZTS is a severe problem, as is introduced in section 2.1.3. Although tremendous efforts have been made in literature to supply chalcogen sources to suppress the occurrence of the decomposition, a fundamental problem remains in how to attain in-situ mastery of the true P_{S2} over the CZTS surface during the high temperature non-equilibrium annealing process, which is still limiting the effective development of kesterite technology. This is the aim of this work, to be able to monitor P_{S2} and to correlate it to CZTS synthesis during the non-equilibrium annealing process. Lastly, it has been demonstrated in this work that high V_{oc} beyond 700 mV can be achieved using high P_{S2}, including a record V_{oc} of 783 mV published for CZTS solar cells so far. The preliminary best solar cell based on the non-optimized CdS buffer during this thesis work is 7.9%,

which is prepared under high P_{S2}. The device parameters in specific are V_{oc} of 691 mV, J_{sc} of 17.0 mA/cm^2, FF of 66.9% and PCE of 7.9%.

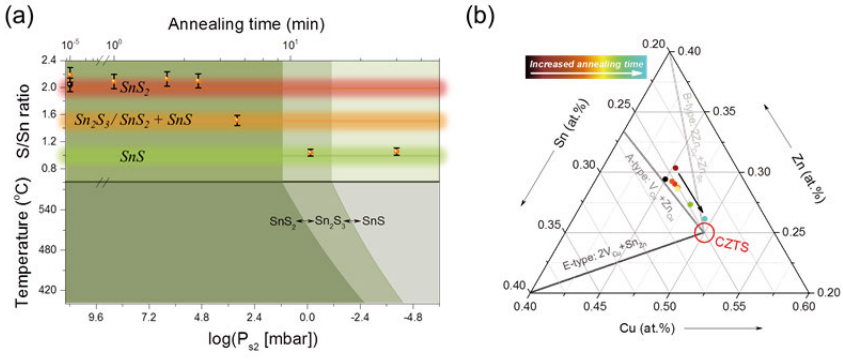

Figure 23. (a) S/Sn ratio, determined by EDS, of the annealed Sn-S films. The colored lines show the S/Sn ratios of possible Sn-S phases accordingly (upper). The black dot represents the precursor. Pressure-temperature phase diagram of Sn-S system (bottom). The boundary of the upper and bottom graphs represents the performed annealing temperature at 580 °C in this work. (b) Tri-plot of the cation composition of the annealed CZTS films prepared with different dwell times under the same annealing process;

The physico-chemical process behind the CZTS decomposition is the reduction from Sn(IV) to Sn(II). In another word, this is analogous to the phase transformation from SnS_2 to SnS. In principle, CZTS can be regarded as the formation from SnS_2, ZnS and Cu_2S. As a result, we can use the SnS_2 film as the monitoring material to know if the P_{S2} is large enough to support CZTS formation or keep it stable (at least, an upper limit for P_{S2} will be found). The results in *Figure 23a* show that besides the dwell time, the dynamic P_{S2} is another important factor in the non-equilibrium annealing. As annealing time continues, P_{S2} apparently drops within a surprisingly short time, driving the SnS_2 to decompose to Sn_2S_3 and SnS within 5 min and 13 min, respectively. This clearly suggests that our annealing atmosphere is very dynamic. The reason for this can be, e.g. the design of our graphite box to preserve the chalcogen vapor. On one hand, the cap of the graphite box is designed with a hole with 2mm in diameter in order to pump out the ambient air prior to the annealing process. On the other hand, this design will allow the equilibration of the pressure between the graphite box and the entire annealing furnace. Since there will be higher sulfur vapor pressure in the graphite box (as calculated) during annealing at 580 °C, than the total pressure in the furnace when the annealing starts, the P_{S2} in the graphite box will decrease due to the leakage tendency.

Furthermore, we looked into the time resolved P_{S2} dependence of CZTS samples that were annealed in the same annealing process as SnS_2 films. In

paper V, we thoroughly investigated the annealed CZTS films from the perspectives of secondary phase formation and defect formation that could possibly be stimulated by either diffusion process (annealing time dependence) or P_{S2} evolution (P_{S2} dependence). With complementary characterizations of Raman and XRD, we can confirm that only Sn-S and ZnS are the formed secondary phases alongside CZTS. Since the initial composition of Zn/Sn is close to 1, and the SnS_2 phase is formed earlier than the ZnS phase when the annealing starts at 0min, this means that CZTS initially prefers Zn rich composition. The compositional plot derived from EDS measurement is displayed in *Figure 23b*. The measurement was attempted on an area presenting no visible secondary phases. It is notable that with increasing annealing time, the CZTS tends to lose Zn content much more than Sn due to the gradual ZnS segregation. Apart from the CZTS film annealed for 0min, the Sn content is also prone to decrease over annealing time partly due to the formation of the SnS_2 phase as well as the later CZTS decomposition. These combined effects cause the composition of CZTS film to end up close to stoichiometry as annealing time was increased, which results in the defect chemistry in CZTS changing at the same time (see *Figure 23b*).

The major question in this work is which variable, i.e. annealing time or P_{S2}, dominates the quality of CZTS during the non-equilibrium annealing process. Assuming the dwell time (maximum is only 40 min in this study) is the paramount for the annealing process (we also neglect the cooling process because the cooling rate remains constant), it is expected that the SnS_2 secondary phase should remain unchanged, and the ZnS secondary phase can precipitate from CZTS film but not grow drastically. Simultaneously, the defect formation is not anticipated to vary significantly, which can be reflected by the ordering parameters. This is owing to that the amount and the state of secondary phases as well as the CZTS composition should only depend on initial composition of CZTS film. Nevertheless, this anticipation is all contrary to our observations. Therefore, based on the discussion in Paper V, we conclude that P_{S2} is a critical factor beyond the annealing time in our annealing process. According to the monitoring material in the annealing process, sufficiently high P_{S2} can only be preserved for annealing time shorter than 3 min, and the CZTS decomposition already occurs in our baseline annealing process of 13 min.

To demonstrate the influence of P_{S2} on the device, solar cells prepared after annealing CZTS with different dwell times were compared, including 1min–high P_{S2}, 40 min-low P_{S2} and reference-13 min. It is shown that high V_{oc} (above 700 mV) of the solar cell can be achieved for 1min-high P_{S2} process, with an overall efficiency of 6-7%. This increase of V_{oc} agrees well with the increase of the CZTS bandgap energy (of above 1.56 eV according to QE edge) which could be facilitated by the changed defect chemistry (see Paper

V). With an additional optimized cooling process to promote the Cu/Zn ordering, we can further boost V_{oc} up to 783 mV, with an overall efficiency above 7%. This strongly supports the importance of controlling P_{S2} to better optimize the CZTS quality with controlled opto-electronic properties.

7.5 Surface compounds on CZTS thin films and their effects on solar cells (Paper VI and VII)

CZTS surface quality is crucial for CZTS thin film solar cells since it is the foundation to create the CdS/CZTS interface. Although the chemical deposition method of CdS is widely used to develop this interface, it is interesting to note that a step of "wet chemical cleaning", with KCN etching being most common, prior to CBD-CdS is still often performed. The role of KCN etching is still under debate. Several reasons were proposed such as modification of surface composition [103, 104] and removal of secondary phases [105]. The aim of this section is to understand the surface chemistry of the CZTS thin film after the annealing process, as well as its influence on the final solar cells.

7.5.1 Influence and evolution of Na related surface compounds

Because of the high annealing temperature for CZTS synthesis, it is highly anticipated that the CZTS surface accumulates Na-related compounds. This is due to the fact that Na is released from SLG substrate to be incorporated into CZTS film during the absorber synthesis. Nevertheless, studies regarding Na-related surface compounds on CZTS are still very rare, and this will be the concern for Paper VI.

Figure 24 shows XPS results of the time resolved air exposure (AE) treatment on annealed CZTS films. As to cations, it can be observed that the only XPS signal of Na 1s gradually increases over time while all the rest tend to decrease as the AE time advances. Turning to the anions, it can be seen that the S 2p peak has a significant evolution over AE time, which includes a decrease of the peak of S^{2-} ion accompanied by a steady increased peak of SO_4^{2-} ion over AE time. Herein, the peak of SO_3^{2-} ion only showed up quickly and vanished after a short AE time of 1.5 h. The XPS results, in combination with the thermodynamic data in Paper VI, lead us to conclude that Na-related compounds are indeed formed on CZTS surface. Apart from Na_2CO_3, this involves a gradual phase transformation from Na_xS to Na_2SO_3 and ultimately to Na_2SO_4.

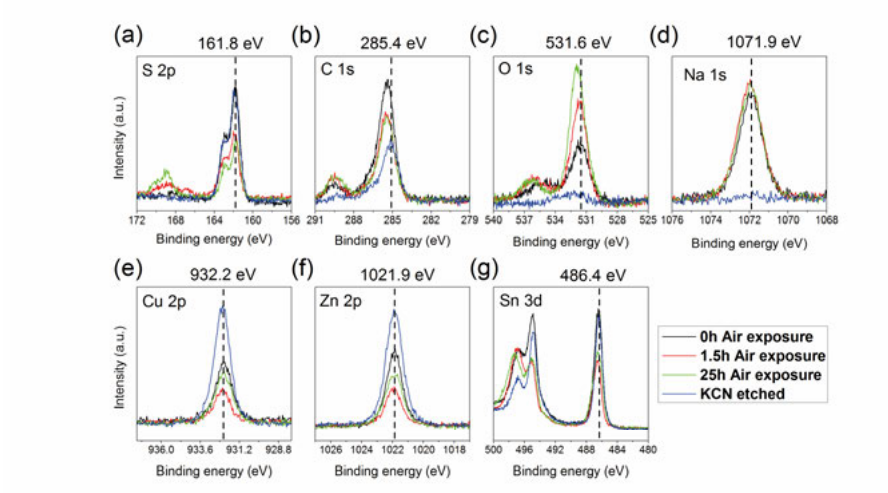

Figure 24. XPS of the surface of CZTS film that is air exposed with different durations. Reprinted from permission of [45]. Copyright ©2016, American Chemical Society

Furthermore, it is observed that the Na-S(-O) compounds can substantially affect the growth of the CdS film, when the CZTS films were directly immersed into chemical bath after different AE time. With additional experiments by depositing individual Na_xS, Na_2SO_3 and Na_2SO_4 layers on identical CZTS samples that were KCN cleaned, we demonstrate that Na_xS compounds are harmful for a controlled growth of CdS film, while Na_2SO_3 and Na_2SO_4 compounds are harmless. The negative influence of the Na_xS compound could be due to the fact that it alters the local pH close to the solution/CZTS interface in the chemical bath, or that it accelerates CdS precipitates, which shifts the atom-by-atom growth of CdS film to agglomeration growth of CdS (see elucidation in Paper VI or section 3.4). The discovery of the influence of the Na-S(-O) compounds inspires us to investigate the role of KCN etching. We find that the actual role of KCN etching for our Cu-poor and Zn-rich CZTS film is to clean the Na_xS compounds and to remove some ZnS secondary phases from the surface of CZTS film, as partly indicated in *Figure 24*.

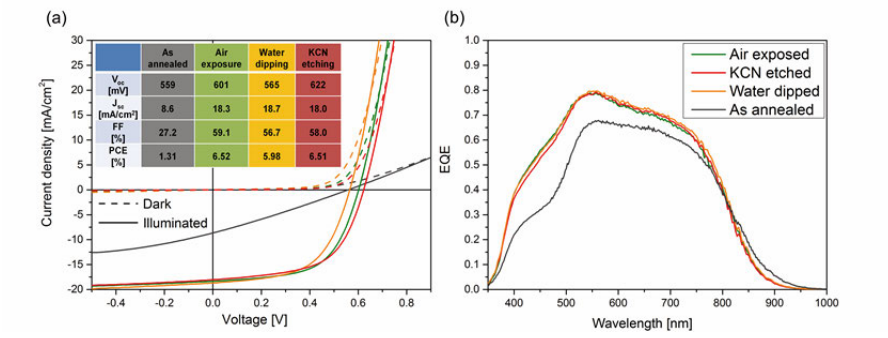

Figure 25. (a) J-V characteristics and (b) EQE of the solar cells prepared from different surface treatments. Reprinted from permission of [45]. Copyright ©2016, American Chemical Society

Lastly, to demonstrate the importance of removal of the Na_xS compound on CZTS surface, solar cells were prepared with different surface treatments on identical annealed CZTS films, as seen in *Figure 25*. It is obvious that either AE treatment (dry method) or wet clean (wet method) on the annealed CZTS surface can improve the solar cell performance.

7.5.2 Air annealing treatment on CZTS surface

An alternative way to increase the rate of the oxidation process (i.e. to convert Na_xS to Na_2SO_4) for the CZTS surface modification is to perform an air annealing treatment. This will be discussed in correlation to Paper VII.

Effect from air annealing temperature

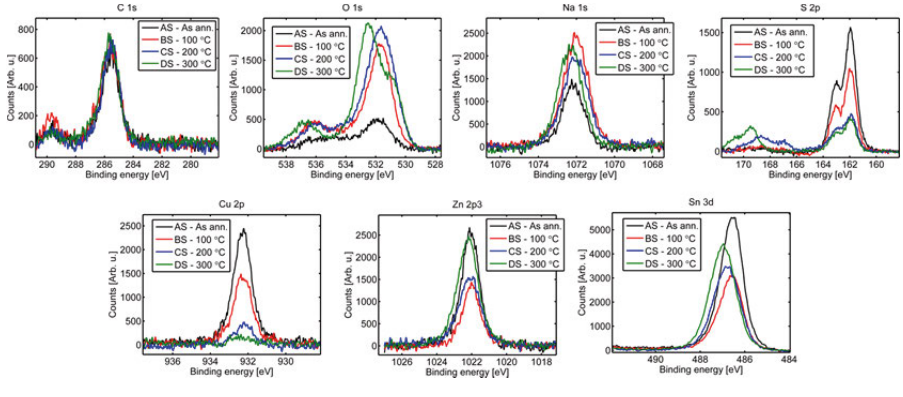

Figure 26. XPS of the CZTS surface that is air annealed at different temperature

Figure 26 shows the XPS spectra of the annealed CZTS films that were air annealed for 10min at temperatures of 100 to 300 °C. At 100 °C, it can be

observed that the XPS peak intensity of S 2p, Zn 2p, Sn 3d was decreased while the XPS peak intensities of O 1s and Na 1s were increased. Besides, the carbonate peak at 289.6 eV for C 1s also showed up at this temperature. This is an implication that a layer of Na carbonate is likely to form on CZTS surface since all Cu, Zn, Sn and S elements seems to decrease with a similar extent. When the air annealing temperature was increased to 200 °C, it is interesting to find that XPS peak intensity of Zn 2p and Sn 3d was increased accompanied by a slight peak broadening, simultaneously, the XPS peak intensity of Na 1s was decreased. In addition, the sulfite peak at 166.9 eV next to the main sulfide peak for S 2p appeared, while the carbonate peak for C 1s was gone. The development of the XPS spectra suggests that Zn and Sn based oxides alongside the metal sulfites, e.g. Na_2SO_3, are likely to form when air annealing the CZTS film at 200 °C. At 300 °C, the sulfite compounds (XPS peak at 169.1 eV) were transformed to sulfate phase according to XPS peaks for S 2p. The sulfate phases, likely Na_2SO_4, together with Zn and Sn based oxides nearly covered the entire CZTS surface, because the peak of Cu 2p had almost completely vanished.

Effect from ammonia etching

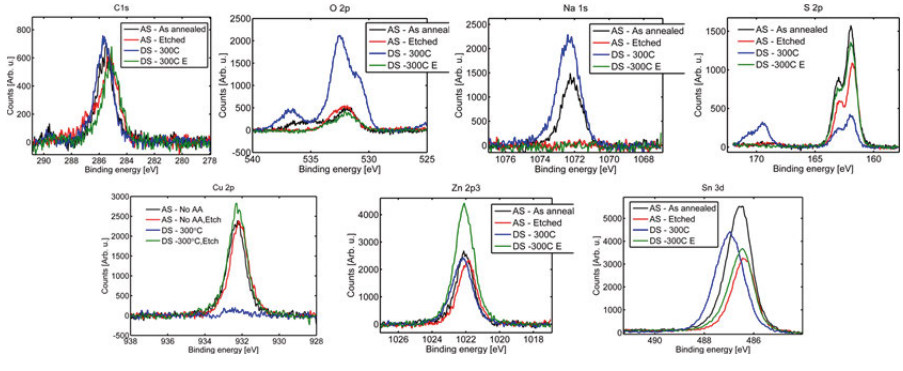

Figure 27. XPS of different CZTS surface that is (un-)treated with ammonia etching

From *Figure 26*, it can be concluded that oxides and sulfate compounds are the most stable phases on CZTS surface when the air annealing was performed at 300°C. It is now interesting to compare the effect of ammonia cleaning on CZTS, inasmuch as ammonia is used as a pH modulator during CBD-CdS process. *Figure 27* shows the XPS comparison of the CZTS films before and after ammonia etching. For air annealed samples before and after etching, it is notable that Na compounds and Zn as well as Sn based oxides were all removed from CZTS surface by looking into peak of S 2p (sulfate), Na 1s, Zn 2p and Sn 3d, at the same time, the XPS peak of Cu 2p becomes apparent. Interestingly, comparing the etched CZTS samples that were prepared with/without air annealing, we found there is an obvious Zn enrich-

ment on CZTS surface, with a less extent to Cu, due to the air annealing treatment. In contrast, the XPS peak intensity of Sn 3d is reduced. The exact reason for this phenomenon is worth further investigation. It may be a result of the initial composition of the CZTS precursor. Since the composition of the studied CZTS film has Cu/(Zn+Sn) and Zn/Sn nearly 1, and we know the P_{S2} loss happening during our baseline annealing could promote CZTS surface decomposition, in which case it is expected that the Sn content could become less close to CZTS surface (Zn/Sn > 1) after annealing. Therefore, the air annealing may exaggerate the Zn rich effect.

A similar result of surface Zn enrichment by air annealing was also reported by Height et al. [106], and it is claimed to be beneficial for the surface bandgap widening of CZTSe, that is terminated with Zn-rich surface, to reduce interface recombination by enlarging the hole barrier [75]. It needs to be noted that the same Zn rich surface also occurs to our CZTSSe samples. However, in CZTSSe, both XPS peaks of Cu 2p and Sn 3d were decreased, which is different from the case for CZTS.

7.5.3 Solar cell performance from air annealing treatment

To further investigate the effect from the surface treatments on the annealed CZTS film, solar cells were fabricated and the device performances are summarized in *Figure 28*. The sulfide devices presented in *Figure 28a* were all fabricated based on KCN etching. However, with the ammonia etching, the device performance in fact showed a similar trend to *Figure 28a* but with overall lower values. As a comparison to sulfide devices, the ammonia etching was done for CZTSSe samples, and the device performances are presented in *Figure 28b*.

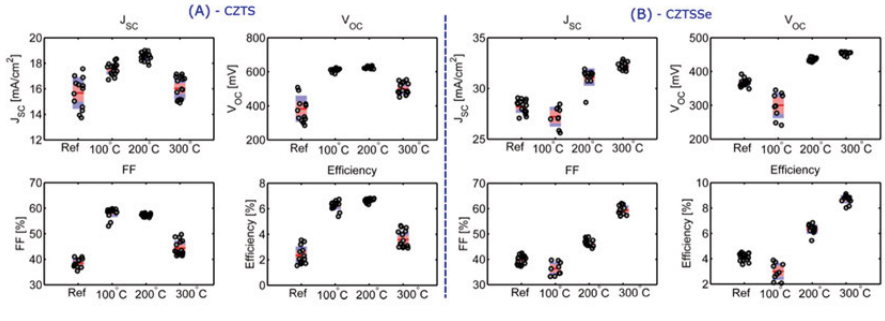

Figure 28. Device performance of the air annealed (a) CZTS and (b) CZTSSe; Before CBD-CdS, the sulfide samples were KCN etched while the sulfo-selenide samples were ammonia etched. Reprinted from [107]. Copyright ©2017, with permission from Elsevier

In *Figure 28a*, the reference device performance is poorer than our normal baseline process, as e.g. seen in Papers II, V and VI. The reason can be that the composition of the CZTS film used in this study has non-optimal value (Cu/Sn = 1.94 and Zn/Sn = 1 while baseline composition typically has Cu/Sn = 1.89, Zn/Sn = 1.1). The air annealing can partly recover the poor reference device behavior, but differing from the CZTSSe device, air annealing at 300°C deteriorated the sulfide solar cells. In *Figure 28b*, the linear relationship between the CZTSSe device and the air anneal temperature (>100 °C) can also be correlated to a decrease of elemental Se that was condensed on CZTSSe surface after the selenization process.

In summary, it is demonstrated that Na-S(-O) compounds play important roles for the surface chemistry of the annealed CZTS thin film. These can change the solution/CZTS interface chemistry during the CBD-CdS. To remove them, two effective routes were presented, i.e air exposure/air annealing (dry process) and wet chemical etching. However, it must be emphasized that the surface modification route using oxidation process can also potentially affect the bulk properties of the CZTS film such as the grain boundary (GB) passivation or variation in chemical composition in the vicinity of GBs [84].

8. Concluding Remarks and Future Work

Conclusion

In general, this thesis was dedicated to developing the two-stage route for CZTS synthesis, and to correlate the quality of CZTS films to the final solar cell performance. In specifics, the thesis work mainly focused on the annealing process for CZTS formation, from the perspective of the formation of secondary compounds. Synthesis of CZTS films with controllable opto-electronic properties at high annealing temperature is challenging due to the chemical instability of CZTS. To attain deeper insight into the effects from the annealing process on CZTS formation, the basic parameters, such as temperature, Ar pressure, ramping rate and cooling rate for the thermal treatment were kept constant, so that it can be used as baseline process. One great advantage of this experimental methodology is to minimize the possible variables during the annealing process. As a result, the primary questions raised for the projects can be concentrated on i) what is the equilibrium state of the annealing process? ii) how will this influence the CZTS properties? iii) will this influence the final solar cells? and iv) how can we improve matters?

It is demonstrated that the reactive co-sputtering process is a powerful deposition method to prepare different binary and ternary materials that are parts of the Cu-Zn-Sn-S system. Upon baseline annealing, the most stable phases can be crystallized from their initial respective metastable states. The results allow us to anticipate the possible secondary phases when we prepare CZTS films with the baseline annealing process (Paper I). Throughout the entire thesis work, we can conclude that only ZnS and Sn-S secondary phases are likely to form when we anneal Cu-poor, Zn-rich CZTS precursors, via XRD, Raman (multiple laser wavelength), SEM-EDS and XRF. These secondary phases can be found on both surface and backside of annealed CZTS films. Additionally, ZnS phases can – but Sn-S phases cannot – be observed in CZTS bulk. This is an important conclusion. Identification of the type of secondary phases as well as their distribution in CZTS film can be directly and indirectly correlated to the quality of CZTS film and final solar cells. The CZTS thickness study well reflected this argument (Paper II). On one hand, the formation of secondary phases in a similar manner among different CZTS thickness can possibly promise comparable CZTS bulk quality. On

the other hand, these secondary phases can result in lateral structural inhomogeneities, which can be bad for solar cells (thin cells in particular).

The impact of the SnS secondary phase on CZTS solar cells is particularly studied with EBIC measurements (Paper III), due to a lack of understanding of its contribution to solar cells. It is found that this phase formed at the CZTS rear can possibly be helpful for CZTS solar cells under the condition that the charge carrier collection depth is comparable to the absorber thickness. This may be a result of a passivation effect. However, it is still inconclusive whether this phase improves overall solar cell performance, since the spontaneous separation of the SnS phase from the annealed CZTS can again suggest that lateral structural homogeneities can be an issue, which may counteract with the benefits from the SnS phase and still limit the solar cell performance. The possible passivation effect was explored by employing an external layer, i.e. Al_2O_3 layer with nano-sized openings on the Mo/SLG substrate, for ultra-thin CZTS solar cells (Paper IV).

The discovery of Sn-S secondary phases is interesting and remarkable, since the formation of SnS directly indicates that our baseline annealing process is not in a steady state. As already concluded from Paper I, P_{S2} during the baseline annealing process drops over time, due to the observation of a phase transformation from SnS_2 to SnS. Alternatively, it also implies that SnS_2 material can be used to monitor the P_{S2} during the annealing process. To confirm this hypothesis, identical CZTS samples were annealed for various durations with SnS_2 films being the monitor material in the same annealing batch, and it is demonstrated in Paper V that beyond annealing time, the P_{S2} is indeed a critical factor that can dominate the material quality of CZTS. It is remarkable to observe that solar cells with V_{oc} beyond 700 mV can be fabricated when CZTS is prepared under high enough P_{S2}, thanks to the information from the monitoring material in the annealing process.

Other secondary compounds that are rarely reported in literature are the Na-related compounds. In particular, Na_xS compounds are anticipated to form on CZTS surface after the annealing process, since Na can be released from SLG and chalcogen vapor is supplied for the CZTS formation. In Paper VI, we demonstrated that Na_xS compounds are indeed likely to form on CZTS surfaces and are harmful for a controlled growth of CBD-CdS, and thereby deteriorate final solar cells. The compounds can be removed by either air exposure/air annealing (dry methods) or etching solution (wet methods). In addition, further study of air annealing at high temperature shows that not only the Na-related phases are transformed on surface, but the CZTS surface also becomes enriched in Zn. The surface Zn enrichment effect could be a reason for an improvement of the CZTSSe solar cell (Paper VII).

Future work

Based on the above conclusions, future work is recommended in the following areas:

i. The annealing process should be modified to provide high P_{S2} for longer annealing times.

ii. The method to monitor the P_{S2} should be improved in order to have better sensitivity for P_{S2} variations.

iii. The compositional effects on CZTS solar cells should be reinvestigated, since the defect chemistry in CZTS bulk can be different due to changes in P_{S2}, and also the formation and distribution of secondary phases could be better controlled if the high P_{S2} during the annealing process can be guaranteed.

iv. Once the CZTS bulk can be improved, the passivation effect as well as the thickness can be reinvestigated and re-optimized.

v. An investigation of Na could be interesting, in order to control the amount of Na_xS compounds on CZTS surface.

vi. The wet cleaning process of Na surface compounds can be further improved, in order to simplify the steps between CBD-CdS (if it is still the focus) and annealing, and avoid the use of environmentally harmful chemicals such as KCN.

In general, as long as sufficient P_{S2} can be maintained during annealing process, investigation of CZTS should be revised. One major impact of the thesis work is the observation of a possible change in defect chemistry of CZTS material due to the change of P_{S2}. Therefore, it is expected that there will be alterations and improvement of several optoelectronic properties of CZTS, such as doping, bandgap, bandgap fluctuations and so forth. This is an important remark. Recent studies have shown that alternative buffers can reduce the interface recombination of the solar cells to improve their V_{oc}. In combination with the enhanced V_{oc} proven in this thesis work, it is strongly foreseen that an aim of over-1000 mV V_{oc} for CZTS solar cells is not unachievable. Annealing CZTS, in one way or another, is similar to cooking Chinese food, in which one has to mix everything to tune its taste, and all of a sudden, "Ah-ha!" The best taste is always the most surprising one. There is much further work to be done to optimize CZTS devices in addition to the presented thesis work. Beyond kesterite, this thesis work also provides a more general solution/reference for better understanding materials that are required to be synthesized in a chalcogen environment with a high temperature annealing process.

Summary in Swedish

Den industriella och teknologiska utvecklingen under de senaste århundradena har möjliggjorts av tillgången av fossila bränslen. Den intensiva användningen av dessa fossila bränslen har samtidigt försatt mänskligheten inför enorma utmaningar som blivit alltmer påtagliga. De fossila bränslena är begränsade och dess utsläpp förorenar luft och atmosfär som riskerar att ställa mänskligheten inför den största utmaningen hittills, den globala uppvärmningen.

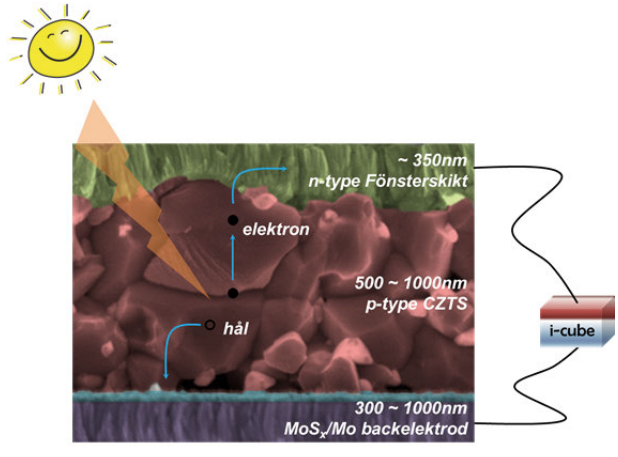

Figure 29. Funktionen hos en tunnfilmssolcell av CZTS.

Solceller, som miljövänlig och förnyelsebar teknologi, spås bli en viktig pusselbit för att uppfylla behovet av elproduktion i takt med att energiomställningen blir alltmer nödvändig, både på kort och lång sikt. Solceller bygger på den fotovoltaiska effekten. Som illustrerat i *Figure 29*, så behöver en solcell absorbera ljus för att kunna generera ett elektron-hål-par i ett halvledarmaterial, laddningsbärarna, den negativa elektronen samt det positiva hålet, fångas upp av fram- respektive bakkontakten, och kan på så sätt nå ut i den externa likströmskretsen och driva elektriska komponenter i kretsen.

I dagsläget dominerar kiselbaserade solceller marknaden. Men, på grund av den låga absorptionskoefficienten för kisel så krävs relativt stor tjocklek för att absorbera allt inkommande ljus, vilket gör materialåtgången stor vid tillverkningen av kiselsolceller. Detta är en anledning till att mer och mer in-

tresse ges till alternativa solcellsteknologier, mest intressanta är solceller av halvledarmaterial med direkt bandgap och hög absorptionskoefficient. Under de senaste åren har kesterit-CZTS fått enorm uppmärkssamhet tack vare att den enbart innehåller i jordskorpan vanligt förekommande ämnen och samtidigt har de eftersträvansvärda halvledaregenskaperna. Dessutom, genom att legera olika kemiska grundämnen, som t. ex. selen och germanium, så går det att skräddarsy egenskaper som bandgap. Tills idag har effektiviteten för kesteritsolceller stadigt ökat till 12,7%. Ytterligare förbättringar krävs alltså för att nå målet på 15% för att bli ett industriellt och kommersiellt gångbart alternativ. Ett nyckelproblem som hindrar utvecklingen av CZTS-solceller är bristen på förståelse för hur sekundära faser som bildas under den nödvändiga värmebehandlingen påverkar CZTS-filmerna. Att öka denna förståelse är det huvudsakliga målet för den här avhandlingen. Dessutom läggs en del fokus på att undersöka och förstå sambandet mellan materialkvalitet och den slutgiltiga solcellsprestandan. För att uppnå de här målen utfördes material- och solcellskarakterisering under kontrollerade experimentförhållanden, mestadels i renrumsmiljö.

De huvudsakliga sekundära faserna som undersökts i den här avhandlingen är tennsulfid (Sn-S) och natriumrelaterade (Na-) kemiska ytföreningar. Det kunde observeras att bildandet av Sn-S-faser kan relateras till sammansättningen av CZTS-filmen och även till dess nedbrytning. De nämnda faserna förekom allt som oftast i gränsskikten i CZTS-solcellerna (se artikel II, III och IV). SnS-fasernas påverkan är olika beroende i vilket gränsskikt det formas i, de som bildas på ytan av CZTS har enbart en försämrande effekt på solcellen, medan de som bildas i det bakre gränsskikten kan bidra till en högre ström. För Na-innehållande ytföreningar så upptäcktes det att Na_xS bör avlägsnas från CZTS-ytan efter värmebehandlingen, detta eftersom det kan ha en väsentlig negativ inverkan på CdS/CZTS-gränsskiktets kvalitet. Både oxidativ behandling och våtkemisk etsning kan avlägsna NaxS-föreingar på CZTS-ytan (artikel VI och VII).

Ytterligare en viktig del i den här avhandlingen är att kontrollera och undersöka effekten av svavelpartialtrycket (P_{S2}) under värmebehandlingen. Detta görs för att undersöka Sn-S-fasomvandlingen (artikel I och V). Det visas att det undersökta P_{S2} väl korrelerar med en serie förändringar i materialkvalitén hos CZTS. Slutligen så visades att en hög öppenkrets-spänning (V_{oc}) för CZTS-solceller kan åstadkommas genom att kontrollera P_{S2} under värmebehandlingen.

Sammanfattningsvis, den här avhandlingen understryker vikten av att kontrollera P_{S2} för att i sin tur kunna kontrollera faserna i CZTS. För att kunna

syntetisera CZTS med kontrollerad bulkkvalitet så är det av högsta vikt att sträva efter förbättringar i gränsskiktet för kesteritbaserade teknologier. Slutligen, upptäckterna i den här avhandlingen kan bli en viktig vägledning för tunnfilmsforskningen, gränsskiktsanalys och förståelse för halvledarmaterial och hur dessa kan förbättras.

Acknowledgement

This PhD means a lot to me, it is the process for me not only to explore knowledge, but also to improve self-perception of my own. More than that, the friendship and relationship I could embrace with in life and at work during past years are great and invaluable for me. This PhD voyage is gorgeous, during which I could meet so many lovely people. Without your contributions, I would not come to this destination and it won't be me. I would like to sincerely thank all people who are willing to come to my life and make it wonderful.

- ***Lotten***, thank you for accepting me as your PhD student to show your first believe in me. In the past years, thank you so much for your endurance, criticism, openness and support. My self-progress benefiting from these aspects is far beyond words. To me, you are not only a true supervisor but also a real mentor.
- ***Jonathan***, it is a great pleasure for me to have you as my co-supervisor. Thank you very much for always showing your interests in my work. Your critical insights and discussions in my projects really inspire me a lot. Thank you for always being patience to improve my "Chi-glish" writing style to be much more professional. I will feel guilty if I could not improve my written English into higher levels.
- ***Marika***, I am so impressed by your passion on solar energy research and your knowledge on solar field. Thank you for always showing the smiling face and willing to solve my problems. Without you and Lotten's help at the beginning of my PhD, I would probably be "struggling" to get back to Sweden. ☺
- ***Uwe***, thank you for your great help with my work in the past years, the first code flashed in my mind when I encountered troubles in cleanroom is always "U-W-E". Thank you for all your great support and patience in these years, and also thank you for preserving the culture of "Friday beer" in FTE.

I also would like to extend my gratitude to my lovely colleagues at ÅSC in the past and at present, which makes my life and work full of fun. ***Bart***, thank you for the great collaboration, your enthusiasm and energy on research seems inexhaustible, which inspires me a lot. ***Marie*** and ***Marc***, thank you for bringing me into the solar world and supporting me to continue with a PhD education. ***Christopher***, thank you for your humor and positive atti-

tudes towards everything. Thanks for showing me how to make cheese cake. I will let you taste mine, and I promise non-toxic! ***Adam***, it feels really relaxable being with you and thank you for always being patient, open and positive. Thanks for your snowboard school. Very first time snowboarding in my life, not too bad hah! ***Tove***, thanks for introducing me to running process for CZTS precursors and always open to help in the lab. ***Jes***, thank you for your nice companies for the conferences and meetings we have been together, and thanks for your help to my work whenever I need. ***Sven*** and ***Katharina***, thank you for your fika and discussions on culture differences, and many time helps in the cleanroom. ***Alexandra***, ***Svente*** and ***Nils***, Thanks for the great arrangement for the Oslo trip, it was fun! Thank you for your inputs during CZTS meetings. ***Jan*** and ***Tobias***, thank you for your discussions on device physics and XRD. ***Oleksandr*** and ***Carl***, it is nice to work with you and thank you for all your discussion in and outside work. ***Olivier***, thank you for your funny remarks and nice insights into the scientific questions, thanks for help with EBIC setup. Past and present solar cell group members (***Viktor, Erik, LI Shuyi, Fredrik G, Timo, Johan, Filippo, Fredrik L, Nina, Piotr*** and ***Dorothea)*** as well as Solibro fellas ***(Uwe, Daniel, Johan*** and ***Erik)***, thank you all to add a nice work environment, and thank you for your support and help to my work.

Furthermore, I would like to thank my wonderful FTE and Ångström colleagues. ***Shili***, for your effort to have the division run smoothly, and for your suggestions and comments on my work. ***Jörgen***, for your effort to manage PhD study and for your patience to explain me with the device physics. ***WEN Chenyu*** and ***CHEN Xi***, for your great company during the work. ***LI Lingguang***, ***Melina*** and ***Shabnam***, for getting me familiar with the life in FTE as well as Uppsala. All FTE fellas, for sharing experience during/off work, particular PhD students (***Malkolm, Lukas, XU Xingxing, ZHAO Jie, ZENG Shuangshuang*** and ***Patrick***). ***Victoria***, ***Jan-åke*** and ***Farhad***, thank you for maintaining the tools and chemicals. ***Ingrid*** and ***Jonathan***, thank you for resolving many times of my problems on computer and administration.

I also would like to give the special thanks to the EU-KESTCELLS project. Thank you, ***Edgardo***, to manage to get such big project run smoothly, and ***Josémi***, thank you for your great patience and assistance to always kindly remind us about the seemingly endless documents we need to prepare for the project, and the arrangement for the ESADE business school. In addition, it is so wonderful to meet so many people expertizing in solar cells in this European project, and it feels so cool to grow together with young researchers. Thank you ***Ian*** and ***Pepe***, ***Thomas***, ***Alex*** and ***Stephan***, ***Rémi*** and ***Jose Maria***, for the great help for my secondments, and the nice collaborations.

I would like to give big hugs to my friends who greatly support me and make my life wonderful no matter where I am. ***ZHANG Da*** and ***SONG Man***, thank you for your selfless friendship during the past years, which enables my life being comfortable and fruitful in Uppsala. ***CHEN Song***, ***JIAO Mingzhi, ZHANG Peng***, and ***CAI Shengzhen***, thank you for your great companies and sharing me with laughs and sufferings. ***Bo, Teng*** and ***Siyuan***, thank you for always giving me your greatest cheering. ***Jie, Minxian*** and ***Huayue***, thank you for offering me your warmest helps whenever I need. I am also very grateful for the friendships from ***YANG Weijia, WANG Zhaohui, HUANG Wen, WANG Shihuai, LI Hu, GUO Meiyuan, WU Di, SHI Liyang, CHU Jiangtao, WANG Baochang, LAN Xin, SUN Fengzhen, SONG Yang, XU Changgang, WEI Wenjing, WEI Wei, Jan, Michael*** and ***Gannish***. Thank you all my fellas, without you being surrounding me the life will surely fade its color.

Last but not least, I would like to give my deepest gratitude to my family. To my parents, thank you so much for being able to understand me and being supportive to what I choose. To my beloved wife, Xiaowen, thank you so much for your love and warmth. Without you, I could not imagine how I could manage to keep life balanced. It is so wonderful to experience together with you hand by hand no matter what.

在这里我要感谢我的家人，感谢我的父母，感谢你们可以理解并尊重我的选择，感谢你们一直以来对我的支持和信任。感谢我的挚爱，晓文，感谢你的一路陪伴，我已无法想像没你的日子会是如何的暗无天日，因为你的存在让我的生活充满了耀眼阳光，很高兴可以与你携手一同走过并迈向未来。

Now, it is time to close this diary…

REN Yi (任毅)

Uppsala, 2017-02-15

Appendixes

Appendix I

Table A1. Gibbs free energy of formation of various possible chemical reactions on CZTS at 580 °C

Chemical Reaction	$\Delta_r G_m$ (kJ/mol)	Ref
$Mo(s) + S_2(g) \Leftrightarrow MoS_2(s)$	-90.0	[108]
$Mo(s) + SnS_2(s) \Leftrightarrow MoS_2(s) + SnS(s)$	-34.9	[46]
$Cu_2ZnSnS_4(s) \Leftrightarrow Cu_2S(s) + ZnS(s) + SnS_2(s)$	14.2	[109]
$2Cu_2ZnSnS_4(s) + Mo(s) \Leftrightarrow 2Cu_2S(s) + 2ZnS(s) + 2SnS(s) + MoS_2(s)$	-6.6	[46, 109]

Table A2. State of the art kesterite thin film solar cells, with the absorber produced from various processes

Process	Material	Method	Sub. T (°C)	Gas	**PCE (%)**	Voc (mV)	Jsc (mA/cm^2)	FF (%)	Buffer	Ref
				One-stage						
Vacuum	CZTSe	Co-evaporation	450	Se vapor	**9.2**	377	37.4	64.9	CdS	[25]
				Two-stage process						
Vacuum	CZTS	Co-evaporation	150+570	S vapor	**8.4**	661	19.5	65.8	CdS	[72]
	CZTSe	Co-evaporation	150+590	Se vapor	**11.6**	423	40.6	67.3	CdS	[50]
	CZTSe	Sputtering	450	H_2Se	**10.4**[a]	395	39.7	66.2	CdS	[110]
	CZTS	React. Co-sputtering	180+560	H_2S+Svapor	**7.9**	667	19.6	60.0	CdS	[22]
	CZTS	Comp. Co-sputtering	250+580	S vapor	**9.0**	679	21.6	61.4	ZnSnO	[111]
					7.1	783	14.1	63.2	CdS	This work
	CZTSe	Sputtering	RT+550	Se vapor+Sn powder	**10.1**	453	33.3	66.8	CdS	[112]
	CZTS	Co-sputtering	RT+560	S vapor	**9.2**	748	19.5	63.2	CdZnS	[76]
	CZTS	Co-sputtering	RT+560	S vapor + SnS	**8.8**	667	19.5	67.5	CdS	[29]
	CZTS	Sputtering	RT+550+ 550-400	H_2S	**8.8**	710	17.5	71.0	Anneaed CdS	[39]
	CZTS	Sputtering/Evaporation	Unknown	Unknown	**9.2**	708	21.6	60.1	InS/CdS	[113]
	CZTS	Monograin	740+740	S atmosphere	**9.1**	759	19.0[b]	63.0	CdS	[33]
	CZTSSe	Sputtering	300+510	S/SeS_2	**12.3**	521	35.0	67.2	CdS	[114]
Non-Vacuum	CZTSSe	Hydrazine+Spin coating	> 500	Unknown	**12.6**	513	35.2	69.8	CdS	[40]
	CZTSSe	Solution+Sping coating	320+300 +500	Se vapor	**11.2**	479	36.5	63.8	CdS	[42]
	CZTSSe	Ink+Spray	Unknown	Se contained	**10.8**	510	32.5	65.0	CdS	[115]

a. With antireflective coating; b. Area is corrected based on grain size;

References

[1] S.M.Sze, K.K. NG, Physics of semiconductor devices, John Wiley & Sons, Inc., 2007.
[2] M.A. Green, K. Emery, Y. Hishikawa, W. Warta, E.D. Dunlop, D.H. Levi, A.W.Y. Ho-Baillie, Solar cell efficiency tables (version 49), Prog.Photovolt:Res.Appl., (2016).
[3] L.M. Peter, Towards sustainable photovoltaics: the search for new materials, Philosophical Transactions of the Royal Society A: Mathematical, Physical and Engineering Sciences, 369 (2011) 1840.
[4] S.A.S. Corp., http://www.slideshare.net/kwoodwardsoam/sac-april-2012-presentation-update-v4, in, April 2012
[5] J. Gambogi, https://minerals.usgs.gov/minerals/pubs/commodity/rare_earths/myb1-2014-raree.pdf, in, 2014.
[6] www.slv.se, in.
[7] C. Persson, Electronic and optical properties of Cu_2ZnSnS_4 and $Cu_2ZnSnSe_4$, J. Appl. Phys., 107 (2010) 053710.
[8] I. Kentaro, N. Tatsuo, Electrical and optical properties of stannite-type quaternary semiconductor thin films, Jpn. J. Appl. Phys., 27 (1988) 2094-2097.
[9] S. Chen, X.G. Gong, A. Walsh, S.-H. Wei, Crystal and electronic band structure of Cu_2ZnSnX_4 (X=S and Se) photovoltaic absorbers: First-principles insights, Appl. Phys. Lett., 94 (2009) 041903.
[10] S. Schorr, H.-J. Hoebler, M. Tovar, A neutron diffraction study of the stannite-kesterite solid solution series, Eur. J. Mineral., 19 (2007) 65-73.
[11] S. Chen, A. Walsh, X.-G. Gong, S.-H. Wei, Classification of Lattice Defects in the Kesterite Cu_2ZnSnS_4 and $Cu_2ZnSnSe_4$ Earth-Abundant Solar Cell Absorbers, Adv. Mater., 25 (2013) 1522-1539.
[12] V. Kosyak, N.B. Mortazavi Amiri, A.V. Postnikov, M.A. Scarpulla, Model of native point defect equilibrium in Cu_2ZnSnS_4 and application to one-zone annealing, J. Appl. Phys., 114 (2013) 124501.
[13] L.E. Valle Rios, K. Neldner, G. Gurieva, S. Schorr, Existence of off-stoichiometric single phase kesterite, J. Alloys Compd., 657 (2016) 408-413.
[14] S. Schorr, G. Gonzalez-Aviles, In-situ investigation of the structural phase transition in kesterite, physica status solidi (a), 206 (2009) 1054-1058.

[15] J.J.S. Scragg, L. Choubrac, A. Lafond, T. Ericson, C. Platzer-Björkman, A low-temperature order-disorder transition in Cu_2ZnSnS_4 thin films, Appl. Phys. Lett., 104 (2014) 041911.
[16] K. Rudisch, Y. Ren, C. Platzer-Björkman, J. Scragg, Order-disorder transition in B-type Cu_2ZnSnS_4 and limitations of ordering through thermal treatments, Appl. Phys. Lett., 108 (2016) 231902.
[17] M. Paris, L. Choubrac, A. Lafond, C. Guillot-Deudon, S. Jobic, Solid-State NMR and Raman Spectroscopy To Address the Local Structure of Defects and the Tricky Issue of the Cu/Zn Disorder in Cu-Poor, Zn-Rich CZTS Materials, lnorg. Chem., 53 (2014) 8646-8653.
[18] P. Zawadzki, A. Zakutayev, S. Lany, Entropy-Driven Clustering in Tetrahedrally Bonded Multinary Materials, Physical Review Applied, 3 (2015) 034007.
[19] I.D. Olekseyuk, I.V. Dudchak, L.V. Piskach, Phase equilibria in the Cu_2S–ZnS–SnS_2 system, J. Alloys Compd., 368 (2004) 135-143.
[20] Y. Ren, J.J. Scragg, T. Ericson, T. Kubart, C. Platzer-Björkman, Reactively sputtered films in the Cu_xS–ZnS–SnS_y system: From metastability to equilibrium, Thin Solid Films, 582 (2015) 208-214.
[21] J.J. Scragg, T. Ericson, T. Kubart, M. Edoff, C. Platzer-Björkman, Chemical Insights into the Instability of Cu_2ZnSnS_4 Films during Annealing, Chem. Mater., 23 (2011) 4625-4633.
[22] J.J. Scragg, T. Kubart, J.T. Wätjen, T. Ericson, M.K. Linnarsson, C. Platzer-Björkman, Effects of Back Contact Instability on Cu_2ZnSnS_4 Devices and Processes, Chem. Mater., 25 (2013) 3162-3171.
[23] H. Xie, M. Dimitrievska, X. Fontané, Y. Sánchez, S. López-Marino, V. Izquierdo-Roca, V. Bermúdez, A. Pérez-Rodríguez, E. Saucedo, Formation and impact of secondary phases in Cu-poor Zn-rich $Cu_2ZnSn(S_{1-y}Se_y)_4$ ($0 \leqslant y \leqslant 1$) based solar cells, Sol. Energy Mater. Sol. Cells, 140 (2015) 289-298.
[24] A. Redinger, D.M. Berg, P.J. Dale, S. Siebentritt, The consequences of kesterite equilibria for efficient solar cells, J. Am. Chem. Soc., 133 (2011) 3320-3323.
[25] I. Repins, C. Beall, N. Vora, C. DeHart, D. Kuciauskas, P. Dippo, B. To, J. Mann, W.-C. Hsu, A. Goodrich, R. Noufi, Co-evaporated $Cu_2ZnSnSe_4$ films and devices, Sol. Energy Mater. Sol. Cells, 101 (2012) 154-159.
[26] J.J. Scragg, T. Ericson, X. Fontané, V. Izquierdo-Roca, A. Pérez-Rodríguez, T. Kubart, M. Edoff, C. Platzer-Björkman, Rapid annealing of reactively sputtered precursors for Cu_2ZnSnS_4 solar cells, Prog.Photovolt:Res.Appl., 22 (2012) 10-17.
[27] M. Mousel, T. Schwarz, R. Djemour, T.P. Weiss, J. Sendler, J.C. Malaquias, A. Redinger, O. Cojocaru-Mirédin, P.-P. Choi, S. Siebentritt, Cu-Rich Precursors Improve Kesterite Solar Cells, Adv. Energy Mater., 4 (2014).
[28] G. Brammertz, Y. Ren, M. Buffière, S. Mertens, J. Hendrickx, H. Marko, A.E. Zaghi, N. Lenaers, C. Köble, J. Vleugels, M. Meuris, J.

Poortmans, Electrical characterization of $Cu_2ZnSnSe_4$ solar cells from selenization of sputtered metal layers, Thin Solid Films, 535 (2013) 348-352.
[29] F. Liu, C. Yan, J. Huang, K. Sun, F. Zhou, J.A. Stride, M.A. Green, X. Hao, Nanoscale Microstructure and Chemistry of Cu_2ZnSnS_4/CdS Interface in Kesterite Cu2ZnSnS4Solar Cells, Adv. Energy Mater., (2016) 1600706.
[30] H. Katagiri, K. Jimbo, W.S. Maw, K. Oishi, M. Yamazaki, H. Araki, A. Takeuchi, Development of CZTS-based thin film solar cells, Thin Solid Films, 517 (2009) 2455-2460.
[31] T. Ericson, T. Kubart, J.J. Scragg, C. Platzer-Björkman, Reactive sputtering of precursors for Cu_2ZnSnS_4 thin film solar cells, Thin Solid Films, 520 (2012) 7093-7099.
[32] Y. Ren, J.J.S. Scragg, C. Frisk, J.K. Larsen, S.-Y. Li, C. Platzer-Björkman, Influence of the Cu_2ZnSnS_4 absorber thickness on thin film solar cells, physica status solidi (a), 212 (2015) 2889-2896.
[33] K. Timmo, M. Kauk-Kuusik, M. Pilvet, T. Raadik, M. Altosaar, M. Danilson, M. Grossberg, J. Raudoja, K. Ernits, Influence of order-disorder in Cu_2ZnSnS_4 powders on the performance of monograin layer solar cells, Thin Solid Films.
[34] T.K. Todorov, K.B. Reuter, D.B. Mitzi, High-efficiency solar cell with Earth-abundant liquid-processed absorber, Adv. Mater., 22 (2010) E156-159.
[35] L. Guo, Y. Zhu, O. Gunawan, T. Gokmen, V.R. Deline, S. Ahmed, L.T. Romankiw, H. Deligianni, Electrodeposited $Cu_2ZnSnSe_4$ thin film solar cell with 7% power conversion efficiency, Prog.Photovolt:Res.Appl., 22 (2014) 58-68.
[36] G. Brammertz, M. Buffière, Y. Mevel, Y. Ren, A.E. Zaghi, N. Lenaers, Y. Mols, C. Koeble, J. Vleugels, M. Meuris, J. Poortmans, Correlation between physical, electrical, and optical properties of $Cu_2ZnSnSe_4$ based solar cells, Appl. Phys. Lett., 102 (2013) 013902.
[37] R. Mainz, A. Singh, S. Levcenko, M. Klaus, C. Genzel, K.M. Ryan, T. Unold, Phase-transition-driven growth of compound semiconductor crystals from ordered metastable nanorods, Nat Commun, 5 (2014) 3133.
[38] N.S. Homare Hiroi, Hiroki Sugimoto, Development of high efficiency Cu_2ZnSnS_4 solar cells and modules, in: 26th EU PVSEC, 2011.
[39] S. Tajima, T. Itoh, H. Hazama, K. Ohishi, R. Asahi, Improvement of the open-circuit voltage of Cu_2ZnSnS_4 solar cells using a two-layer structure, Applied Physics Express, 8 (2015) 082302.
[40] W. Wang, M.T. Winkler, O. Gunawan, T. Gokmen, T.K. Todorov, Y. Zhu, D.B. Mitzi, Device Characteristics of CZTSSe Thin-Film Solar Cells with 12.6% Efficiency, Adv. Energy Mater., 4 (2014) 1301465.
[41] C.K. Miskin, W.-C. Yang, C.J. Hages, N.J. Carter, C.S. Joglekar, E.A. Stach, R. Agrawal, 9.0% efficient $Cu_2ZnSn(S,Se)_4$ solar cells from selenized nanoparticle inks, Prog.Photovolt:Res.Appl., 23 (2014) 654-659.

[42] S.G. Haass, M. Diethelm, M. Werner, B. Bissig, Y.E. Romanyuk, A.N. Tiwari, 11.2% Efficient Solution Processed Kesterite Solar Cell with a Low Voltage Deficit, Adv. Energy Mater., 5 (2015) 1500712.
[43] A. Fairbrother, X. Fontané, V. Izquierdo-Roca, M. Espíndola-Rodríguez, S. López-Marino, M. Placidi, L. Calvo-Barrio, A. Pérez-Rodríguez, E. Saucedo, On the formation mechanisms of Zn-rich Cu_2ZnSnS_4 films prepared by sulfurization of metallic stacks, Sol. Energy Mater. Sol. Cells, 112 (2013) 97-105.
[44] M. Johnson, S.V. Baryshev, E. Thimsen, M. Manno, X. Zhang, I.V. Veryovkin, C. Leighton, E.S. Aydil, Alkali-metal-enhanced grain growth in Cu_2ZnSnS_4 thin films, Energy Environ. Sci., 7 (2014) 1931-1938.
[45] Y. Ren, J.J.S. Scragg, M. Edoff, J.K. Larsen, C. Platzer-Björkman, Evolution of Na—S(—O) Compounds on the Cu_2ZnSnS_4 Absorber Surface and Their Effects on CdS Thin Film Growth, ACS Applied Materials & Interfaces, 8 (2016) 18600-18607.
[46] J.J. Scragg, P.J. Dale, D. Colombara, L.M. Peter, Thermodynamic aspects of the synthesis of thin-film materials for solar cells, Chemphyschem : a European journal of chemical physics and physical chemistry, 13 (2012) 3035-3046.
[47] T. Gershon, C. Hamann, M. Hopstaken, Y.S. Lee, B. Shin, R. Haight, Chemical Consequences of Alkali Inhomogeneity in Cu_2ZnSnS_4 Thin-Film Solar Cells, Adv. Energy Mater., 5 (2015) 1500922.
[48] S. Tajima, R. Asahi, D. Isheim, D.N. Seidman, T. Itoh, M. Hasegawa, K. Ohishi, Atom-probe tomographic study of interfaces of Cu_2ZnSnS_4 photovoltaic cells, Appl. Phys. Lett., 105 (2014) 093901.
[49] J.K. Larsen, J.J.S. Scragg, C. Frisk, Y. Ren, C. Platzer-Björkman, Potential of CuS cap to prevent decomposition of Cu_2ZnSnS_4 during annealing, physica status solidi (a), 212 (2015) 2843-2849.
[50] Y.S. Lee, T. Gershon, O. Gunawan, T.K. Todorov, T. Gokmen, Y. Virgus, S. Guha, $Cu_2ZnSnSe_4$ Thin-Film Solar Cells by Thermal Co-evaporation with 11.6% Efficiency and Improved Minority Carrier Diffusion Length, Adv. Energy Mater., 5 (2015) 1401372.
[51] B. Shin, Y. Zhu, N.A. Bojarczuk, S. Jay Chey, S. Guha, Control of an interfacial MoSe2 layer in $Cu_2ZnSnSe_4$ thin film solar cells: 8.9% power conversion efficiency with a TiN diffusion barrier, Appl. Phys. Lett., 101 (2012) 053903.
[52] J.J. Scragg, J.T. Watjen, M. Edoff, T. Ericson, T. Kubart, C. Platzer-Bjorkman, A detrimental reaction at the molybdenum back contact in $Cu_2ZnSn(S,Se)_4$ thin-film solar cells, J. Am. Chem. Soc., 134 (2012) 19330-19333.
[53] W.-C. Hsu, I. Repins, C. Beall, C. DeHart, G. Teeter, B. To, Y. Yang, R. Noufi, The effect of Zn excess on kesterite solar cells, Sol. Energy Mater. Sol. Cells, 113 (2013) 160-164.
[54] G. Altamura, J. Vidal, Impact of Minor Phases on the Performances of CZTSSe Thin-Film Solar Cells, Chem. Mater., 28 (2016) 3540-3563.

[55] Q. Xu, B. Huang, Y. Zhao, Y. Yan, R. Noufi, S.-H. Wei, Crystal and electronic structures of Cu_xS solar cell absorbers, Appl. Phys. Lett., 100 (2012) 061906.
[56] L.A. Burton, A. Walsh, Phase Stability of the Earth-Abundant Tin Sulfides SnS, SnS_2, and Sn_2S_3, The Journal of Physical Chemistry C, 116 (2012) 24262-24267.
[57] S.-Y. Li, C. Hägglund, Y. Ren, J.J.S. Scragg, J.K. Larsen, C. Frisk, K. Rudisch, S. Englund, C. Platzer-Björkman, Optical properties of reactively sputtered Cu_2ZnSnS_4 solar absorbers determined by spectroscopic ellipsometry and spectrophotometry, Sol. Energy Mater. Sol. Cells, 149 (2016) 170-178.
[58] A. Fairbrother, E. Garcia-Hemme, V. Izquierdo-Roca, X. Fontane, F.A. Pulgarin-Agudelo, O. Vigil-Galan, A. Perez-Rodriguez, E. Saucedo, Development of a selective chemical etch to improve the conversion efficiency of Zn-rich Cu_2ZnSnS_4 solar cells, J. Am. Chem. Soc., 134 (2012) 8018-8021.
[59] H. Xie, Y. Sanchez, S. Lopez-Marino, M. Espindola-Rodriguez, M. Neuschitzer, D. Sylla, A. Fairbrother, V. Izquierdo-Roca, A. Perez-Rodriguez, E. Saucedo, Impact of Sn(S,Se) secondary phases in $Cu_2ZnSn(S,Se)_4$ solar cells: a chemical route for their selective removal and absorber surface passivation, ACS Appl Mater Interfaces, 6 (2014) 12744-12751.
[60] J. Just, M. Nichterwitz, D. Lützenkirchen-Hecht, R. Frahm, T. Unold, Compositional dependence of charge carrier transport in kesterite Cu_2ZnSnS_4 solar cells, J. Appl. Phys., 120 (2016) 225703.
[61] Tove Ericson, Jonathan J. Scragg, Adam Hultqvist, Jörn TimoWätjen, Piotr Szaniawski, Tobias Törndahl, C. Platzer-Björkman, Zn(O,S) buffer layers and thickness variations of CdS buffer for Cu_2ZnSnS_4 solar cells, IEEE Journal of Photovoltaics, 4 (2014) 465-469.
[62] B. Vermang, Y. Ren, O. Donzel-Gargand, C. Frisk, J. Joel, P. Salom, x00E, J. Borme, S. Sadewasser, C. Platzer-Björkman, M. Edoff, Rear Surface Optimization of CZTS Solar Cells by Use of a Passivation Layer With Nanosized Point Openings, IEEE Journal of Photovoltaics, 6 (2016) 332-336.
[63] T. Todorov, J. Olenick, K. AOlenick, O. Gunawan, T. Gershon, C. Sturdevant, L. Yun Seog, C. Liang-yi, S. Guha, Flexible kesterite solar cells on ceramic substrates for advanced thermal processing, in: 2015 IEEE 42nd Photovoltaic Specialist Conference (PVSC), 2015, pp. 1-3.
[64] S. Lopez-Marino, Y. Sanchez, M. Espindola-Rodriguez, X. Alcobe, H. Xie, M. Neuschitzer, I. Becerril, S. Giraldo, M. Dimitrievska, M. Placidi, L. Fourdrinier, V. Izquierdo-Roca, A. Perez-Rodriguez, E. Saucedo, Alkali doping strategies for flexible and light-weight $Cu_2ZnSnSe_4$ solar cells, Journal of Materials Chemistry A, 4 (2016) 1895-1907.
[65] I. Becerril-Romero, S. Giraldo, S. López-Marino, M. Placidi, Y. Sánchez, D. Sylla, A. Pérez-Rodríguez, E. Saucedo, P. Pistor, Vitreous

enamel as sodium source for efficient kesterite solar cells on commercial ceramic tiles, Sol. Energy Mater. Sol. Cells, 154 (2016) 11-17.
[66] J. Márquez, M. Neuschitzer, M. Dimitrievska, R. Gunder, S. Haass, M. Werner, Y.E. Romanyuk, S. Schorr, N.M. Pearsall, I. Forbes, Systematic compositional changes and their influence on lattice and optoelectronic properties of $Cu_2ZnSnSe_4$ kesterite solar cells, Sol. Energy Mater. Sol. Cells, 144 (2016) 579-585.
[67] K. Wang, O. Gunawan, T. Todorov, B. Shin, S.J. Chey, N.A. Bojarczuk, D. Mitzi, S. Guha, Thermally evaporated Cu_2ZnSnS_4 solar cells, Appl. Phys. Lett., 97 (2010) 143508.
[68] C. Frisk, Y. Ren, L. Shuyi, C. Platzer-Björkman, CZTS solar cell device simulations with varying absorber thickness, in: Photovoltaic Specialist Conference (PVSC), 2015 IEEE 42nd, 2015, pp. 1-3.
[69] O. Souhaib, B. Guy, B. Marie, E. Hossam, M. Denis, E. Ounsi, T. Oualid, K. Christine, M. Marc, P. Jef, Study of alternative back contacts for thin film $Cu_2ZnSnSe_4$-based solar cells, J. Phys. D: Appl. Phys., 48 (2015) 035103.
[70] F. Liu, K. Sun, W. Li, C. Yan, H. Cui, L. Jiang, X. Hao, M.A. Green, Enhancing the Cu_2ZnSnS_4 solar cell efficiency by back contact modification: Inserting a thin TiB_2 intermediate layer at Cu_2ZnSnS_4/Mo interface, Appl. Phys. Lett., 104 (2014) 051105.
[71] F. Zeng, K. Sun, L. Gong, L. Jiang, F. Liu, Y. Lai, J. Li, Back contact-absorber interface modification by inserting carbon intermediate layer and conversion efficiency improvement in $Cu_2ZnSn(S,Se)_4$ solar cell, physica status solidi (RRL) - Rapid Research Letters, 9 (2015) 687-691.
[72] O.G. Byungha Shin, Yu Zhu, Nestor A. Bojarczuk, S. Jay Chey, Supratik Guha, Thin film solar cell with 8.4% power conversion efficiency using an earth-abundant Cu_2ZnSnS_4 absorber, Prog.Photovolt:Res.Appl., 21 (2013) 72-76.
[73] G. Brammertz, S. Oueslati, M. Buffière, J. Bekaert, H.E. Anzeery, K.B. Messaoud, S. Sahayaraj, T. Nuytten, C. Köble, M. Meuris, J. Poortmans, Investigation of Properties Limiting Efficiency in $Cu_2ZnSnSe_4$-Based Solar Cells, IEEE Journal of Photovoltaics, 5 (2015) 649-655.
[74] T. Gokmen, O. Gunawan, T.K. Todorov, D.B. Mitzi, Band tailing and efficiency limitation in kesterite solar cells, Appl. Phys. Lett., 103 (2013) 103506.
[75] I.L. Repins, J.V. Li, A. Kanevce, C.L. Perkins, K.X. Steirer, J. Pankow, G. Teeter, D. Kuciauskas, C. Beall, C. Dehart, J. Carapella, B. Bob, J.S. Park, S.H. Wei, Effects of deposition termination on $Cu_2ZnSnSe_4$ device characteristics, Thin Solid Films, 582 (2015) 184-187.
[76] K. Sun, C. Yan, F. Liu, J. Huang, F. Zhou, J.A. Stride, M. Green, X. Hao, Over 9% Efficient Kesterite Cu_2ZnSnS_4 Solar Cell Fabricated by Using Zn1–xCdxS Buffer Layer, Adv. Energy Mater., (2016) 1600046.
[77] J.J.S. Scragg, J.K. Larsen, M. Kumar, C. Persson, J. Sendler, S. Siebentritt, C. Platzer Björkman, Cu–Zn disorder and band gap fluctuations

in $Cu_2ZnSn(S,Se)_4$: Theoretical and experimental investigations, physica status solidi (b), 253 (2016) 247-254.
[78] G. Rey, T.P. Weiss, J. Sendler, A. Finger, C. Spindler, F. Werner, M. Melchiorre, M. Hála, M. Guennou, S. Siebentritt, Ordering kesterite improves solar cells: A low temperature post-deposition annealing study, Sol. Energy Mater. Sol. Cells, 151 (2016) 131-138.
[79] H. Xie, S. Lopez-Marino, T. Olar, Y. Sanchez, M. Neuschitzer, F. Oliva, S. Giraldo, V. Izquierdo-Roca, I. Lauermann, A. Perez-Rodriguez, E. Saucedo, Impact of Na Dynamics at the $Cu_2ZnSn(S,Se)_4$/CdS Interface During Post Low Temperature Treatment of Absorbers, ACS Appl Mater Interfaces, 8 (2016) 5017-5024.
[80] S.G. Haass, M. Diethelm, C. Andres, Y.E. Romanyuk, A.N. Tiwari, Potassium post deposition treatment of solution-processed kesterite solar cells, Thin Solid Films, 2016, in press.
[81] Z. Su, J.M.R. Tan, X. Li, X. Zeng, S.K. Batabyal, L.H. Wong, Cation Substitution of Solution-Processed Cu_2ZnSnS_4 Thin Film Solar Cell with over 9% Efficiency, Adv. Energy Mater., 5 (2015) 1500682.
[82] A.D. Collord, H.W. Hillhouse, Germanium Alloyed Kesterite Solar Cells with Low Voltage Deficits, Chem. Mater., 28 (2016) 2067-2073.
[83] N. Ross, J. Larsen, S. Grini, L. Vines, C. Platzer-Björkman, Practical limitations to selenium annealing of compound co-sputtered Cu_2ZnSnS_4 as a route to achieving sulfur-selenium graded solar cell absorbers, Thin Solid Films, 623 (2017) 110-115.
[84] K. Sardashti, R. Haight, T. Gokmen, W. Wang, L.-Y. Chang, D.B. Mitzi, A.C. Kummel, Impact of Nanoscale Elemental Distribution in High-Performance Kesterite Solar Cells
JO - Advanced Energy Materials, Adv. Energy Mater., 5 (2015) 1402180.
[85] K. Ernits, C. Neubauer, X. Li, L.H. Wong, D. Meissner, A. Neisser, Improvement of V_{OC} in Cu_2ZnSnS_4 monograin layer solar cells with tin oxide inter-layer, in: Photovoltaic Specialist Conference (PVSC), 2015 IEEE 42nd, 2015, pp. 1-4.
[86] C. Platzer-Björkman, C. Frisk, J.K. Larsen, T. Ericson, S.Y. Li, J.J.S. Scragg, J. Keller, F. Larsson, T. Törndahl, Reduced interface recombination in Cu_2ZnSnS_4 solar cells with atomic layer deposition $Zn_{1-x}Sn_xO_y$ buffer layers, Appl. Phys. Lett., 107 (2015) 243904.
[87] C. Yan, F. Liu, K. Sun, N. Song, J.A. Stride, F. Zhou, X. Hao, M. Green, Boosting the efficiency of pure sulfide CZTS solar cells using the In/Cd-based hybrid buffers, Sol. Energy Mater. Sol. Cells, 144 (2016) 700-706.
[88] T. Gokmen, O. Gunawan, D.B. Mitzi, Minority carrier diffusion length extraction in $Cu_2ZnSn(Se,S)_4$ solar cells, J. Appl. Phys., 114 (2013) 114511.
[89] Steven S. Hegedus, W.N. Shafarman, Thin-Film Solar Cells: Device Measurements and Analysis, Prog. Photovolt: Res. Appl., 12 (2004) 155–176.

[90] A. Pu, F. Ma, C. Yan, J. Huang, K. Sun, M. Green, X. Hao, Sentaurus modelling of 6.9% Cu_2ZnSnS_4 device based on comprehensive electrical & optical characterization, Sol. Energy Mater. Sol. Cells, 160 (2017) 372-381.
[91] Daniel Abou-Raus, Thomas Kirchartz, U. Rau, Advanced Characterization Techniques for Thin Film Solar Cells, Wiley-VCH Verlag GmbH & Co. KGaA, 2011.
[92] C. Frisk, T. Ericson, S.Y. Li, P. Szaniawski, J. Olsson, C. Platzer-Björkman, Combining strong interface recombination with bandgap narrowing and short diffusion length in Cu_2ZnSnS_4 device modeling, Sol. Energy Mater. Sol. Cells, 144 (2016) 364-370.
[93] G. Rey, A. Redinger, J. Sendler, T.P. Weiss, M. Thevenin, M. Guennou, B. El Adib, S. Siebentritt, The band gap of $Cu_2ZnSnSe_4$: Effect of order-disorder, Appl. Phys. Lett., 105 (2014) 112106.
[94] T. Ericson, Reactive sputtering and composition measurements of precursors for Cu_2ZnSnS_4 thin film solar cells, in, Uppsala University, Uppsala, 2013.06.
[95] M. Nichterwitz, Charge carrier transport in $Cu(In,Ga)Se_2$ thin-film-solar-cells studied by electron beam induced current and temperature and illumination dependent current voltage analyses, in, Technischen Universit at Berlin, Berlin, 2012.
[96] B. Bissig, C. Guerra-Nunez, R. Carron, S. Nishiwaki, F. La Mattina, F. Pianezzi, P.A. Losio, E. Avancini, P. Reinhard, S.G. Haass, M. Lingg, T. Feurer, I. Utke, S. Buecheler, A.N. Tiwari, Surface Passivation for Reliable Measurement of Bulk Electronic Properties of Heterojunction Devices, Small, (2016).
[97] A. Fairbrother, V. Izquierdo-Roca, X. Fontané, M. Ibáñez, A. Cabot, E. Saucedo, A. Pérez-Rodríguez, ZnS grain size effects on near-resonant Raman scattering: optical non-destructive grain size estimation, CrystEngComm, 16 (2014) 4120.
[98] M. Dimitrievska, A. Fairbrother, X. Fontané, T. Jawhari, V. Izquierdo-Roca, E. Saucedo, A. Pérez-Rodríguez, Multiwavelength excitation Raman scattering study of polycrystalline kesterite Cu_2ZnSnS_4 thin films, Appl. Phys. Lett., 104 (2014) 021901.
[99] S.v. Duren, R. Yi, J. Scragg, J. Just, T. Unold, Raman spectroscopy study on in-situ monitoring of Cu_2ZnSnS_4 synthesis, in: 2015 IEEE 42nd Photovoltaic Specialist Conference (PVSC), 2015, pp. 1-3.
[100] U. Chalapathi, Y.B.K. Kumar, S. Uthanna, V.S. Raja, Investigations on Cu_3SnS_4 thin films prepared by spray pyrolysis, Thin Solid Films, 556 (2014) 61-67.
[101] J.K. Larsen, S.-Y. Li, J.J.S. Scragg, Y. Ren, C. Hägglund, M.D. Heinemann, S. Kretzschmar, T. Unold, C. Platzer-Björkman, Interference effects in photoluminescence spectra of Cu_2ZnSnS_4 and $Cu(In,Ga)Se_2$ thin films, J. Appl. Phys., 118 (2015) 035307.

[102] B. Vermang, J.T. Watjen, V. Fjallstrom, F. Rostvall, M. Edoff, R. Kotipalli, F. Henry, D. Flandre, Employing Si solar cell technology to increase efficiency of ultra-thin Cu(In,Ga)Se_2 solar cells, Prog Photovolt, 22 (2014) 1023-1029.
[103] M. Bär, B.-A. Schubert, B. Marsen, S. Krause, S. Pookpanratana, T. Unold, L. Weinhardt, C. Heske, H.-W. Schock, Impact of KCN etching on the chemical and electronic surface structure of Cu_2ZnSnS_4 thin-film solar cell absorbers, Appl. Phys. Lett., 99 (2011).
[104] K. Timmo, M. Altosaar, J. Raudoja, M. Grossberg, M. Danilson, O. Volobujeva, E. Mellikov, Chemical Etching of $Cu_2ZnSn(S,Se)_4$ Monograin Powder, Ieee Phot Spec Conf, (2010) 1982-1985.
[105] M. Buffiere, G. Brammertz, S. Sahayaraj, M. Batuk, S. Khelifi, D. Mangin, A.A. El Mel, L. Arzel, J. Hadermann, M. Meuris, J. Poortmans, KCN Chemical Etch for Interface Engineering in $Cu_2ZnSnSe_4$ Solar Cells, ACS Appl Mater Interfaces, 7 (2015) 14690-14698.
[106] R. Haight, X. Shao, W. Wang, D.B. Mitzi, Electronic and elemental properties of the $Cu_2ZnSn(S,Se)_4$ surface and grain boundaries, Appl. Phys. Lett., 104 (2014) 033902.
[107] J.K. Larsen, Y. Ren, N. Ross, E. Särhammar, S.Y. Li, C. Platzer-Björkman, Surface modification through air annealing $Cu_2ZnSn(S,Se)_4$ absorbers, In proof, Thin Solid Films, (2016), in press.
[108] D.R. Fredrickson, M.G. Chasanov, The enthalpy of molybdenum disulfide to 1200 K by drop calorimetry, The Journal of Chemical Thermodynamics, 3 (1971) 693-696.
[109] S.V. Baryshev, E. Thimsen, Enthalpy of Formation for Cu–Zn–Sn–S (CZTS) Calculated from Surface Binding Energies Experimentally Measured by Ion Sputtering, Chem. Mater., 27 (2015) 2294-2298.
[110] S. Oueslati, G. Brammertz, M. Buffière, H. ElAnzeery, O. Touayar, C. Köble, J. Bekaert, M. Meuris, J. Poortmans, Physical and Electrical characterization of high-performance $Cu_2ZnSnSe_4$ based thin film solar cells, Thin Solid Films, (2014).
[111] Tove Ericson, Fredrik Larsson, Tobias Törndahl, Christopher Frisk, Jes K. Larsen, Volodymyr Kosyak, Carl Hägglund, Shuyi Li, C. Platzer-Björkman, Zinc-Tin-Oxide Buffer Layer and Low Temperature Post Annealing Resulting in a 9.0 % Efficient Cd-free Cu2ZnSnS4 Solar Cell, submitted, (2017).
[112] S. Giraldo, M. Neuschitzer, T. Thersleff, S. López-Marino, Y. Sánchez, H. Xie, M. Colina, M. Placidi, P. Pistor, V. Izquierdo-Roca, K. Leifer, A. Pérez-Rodríguez, E. Saucedo, Large Efficiency Improvement in $Cu_2ZnSnSe_4$ Solar Cells by Introducing a Superficial Ge Nanolayer, Adv. Energy Mater., 5 (2015) 1501070.
[113] N.S. Homare Hiroi, Takuya Kato, Hiroki Sugimoto, High Voltage Cu_2ZnSnS_4 Submodules by Hybrid Buffer Layer, in: 27th EU PVSEC, 2012.
[114] K.-J. Yang, D.-H. Son, S.-J. Sung, J.-H. Sim, Y.-I. Kim, S.-N. Park, D.-H. Jeon, J. Kim, D.-K. Hwang, C.-W. Jeon, D. Nam, H. Cheong, J.-K.

Kang, D.-H. Kim, A band-gap-graded CZTSSe solar cell with 12.3% efficiency, Journal of Materials Chemistry A, 4 (2016) 10151-10158.
[115] G. Larramona, S. Levcenko, S. Bourdais, A. Jacob, C. Choné, B. Delatouche, C. Moisan, J. Just, T. Unold, G. Dennler, Fine-Tuning the Sn Content in CZTSSe Thin Films to Achieve 10.8% Solar Cell Efficiency from Spray-Deposited Water-Ethanol-Based Colloidal Inks, Adv. Energy Mater., 5 (2015) 1501404.

Acta Universitatis Upsaliensis

Digital Comprehensive Summaries of Uppsala Dissertations from the Faculty of Science and Technology 1476

Editor: The Dean of the Faculty of Science and Technology

A doctoral dissertation from the Faculty of Science and Technology, Uppsala University, is usually a summary of a number of papers. A few copies of the complete dissertation are kept at major Swedish research libraries, while the summary alone is distributed internationally through the series Digital Comprehensive Summaries of Uppsala Dissertations from the Faculty of Science and Technology. (Prior to January, 2005, the series was published under the title "Comprehensive Summaries of Uppsala Dissertations from the Faculty of Science and Technology".)

Distribution: publications.uu.se
urn:nbn:se:uu:diva-314975

ACTA
UNIVERSITATIS
UPSALIENSIS
UPPSALA
2017